ANL-07/08

Argonne NATIONAL LABORATORY

Hydrogen Separation Membranes Annual Report for FY 2006

Energy Systems Division

About Argonne National Laboratory

Argonne is a U.S. Department of Energy laboratory managed by UChicago Argonne, LLC under contract DE-AC02-06CH11357. The Laboratory's main facility is outside Chicago, at 9700 South Cass Avenue, Argonne, Illinois 60439. For information about Argonne, see www.anl.gov.

Availability of This Report

This report is available, at no cost, at http://www.osti.gov/bridge. It is also available on paper to the U.S. Department of Energy and its contractors, for a processing fee, from:

U.S. Department of Energy
Office of Scientific and Technical Information
P.O. Box 62
Oak Ridge, TN 37831-0062
phone (865) 576-8401
fax (865) 576-5728
reports@adonis.osti.gov

ANL-07/08

Hydrogen Separation Membranes Annual Report for FY 2006

by
U. (Balu) Balachandran
Energy Systems Division, Argonne National Laboratory

contributors
L. Chen, M. Ciocco*, R.D. Doctor, S.E. Dorris, J.E. Emerson, B. Fisher
T.H. Lee, R.P. Killmeyer*, B. Morreale*, J.J. Picciolo, and S.J. Song
Energy Systems Division, Argonne National Laboratory
*National Energy Technology Laboratory

work supported by
U.S. Department of Energy
Office of Fossil Energy, National Energy Technology Laboratory

January 31, 2007

HYDROGEN SEPARATION MEMBRANES
ANNUAL REPORT FOR FY 2006

ARGONNE NATIONAL LABORATORY
Energy Systems Division
9700 South Cass Avenue
Argonne, Illinois 60439

U. (Balu) Balachandran

Contributors:

L. Chen
M. Ciocco*
R. D. Doctor
S. E. Dorris
J. E. Emerson
B. Fisher
T. H. Lee
R. P. Killmeyer*
B. Morreale*
J. J. Picciolo
R. V. Siriwardane*
S. J. Song

January 18, 2007

Work Supported by

U. S. DEPARTMENT OF ENERGY
Office of Fossil Energy, National Energy Technology Laboratory

*National Energy Technology Laboratory

Argonne National Laboratory is a U.S. Department of Energy laboratory managed by UChicago Argonne, LLC, under Contract Number DE-AC-02-06CH11357.

Contents

Figures

Tables

HYDROGEN SEPARATION MEMBRANES -- ANNUAL REPORT FOR FY 2006
ARGONNE NATIONAL LABORATORY

Project Title: Development of Dense Ceramic Membranes for Hydrogen Separation

NETL Project Manager: Richard Dunst

ANL Project PI: U. (Balu) Balachandran

B&R Code/Contract Number: AA-20-15-00-0/FWP 49601

Report Date: January 18, 2007

I. OBJECTIVE

The objective of this work is to develop dense ceramic membranes for separating hydrogen from other gaseous components in a nongalvanic mode, i.e., without using an external power supply or electrical circuitry.

II. HIGHLIGHTS

1. The chemical stability of ANL-3e membranes was tested in coal gasifier-like feed gas at temperatures ≤600°C.

2. The hydrogen flux of an ANL-3e membrane was measured in Argonne's new high-pressure reactor at temperatures up to 900°C and total pressures up to 280 psig. Flux values are consistent with previously measured values.

3. National Energy Technology Laboratory (NETL) ASPEN designs for Texaco and Shell gasifiers were successfully tested to show that the off-gas from the hydrogen membranes could be recycled to the gasifiers without creating convergence problems.

4. The Pd/Pd_4S phase boundary was determined for ANL-3e membranes in feed gas that contained 73% H_2/59-400 ppm H_2S/balance He. Adding small amounts of other components (CO, CO_2, and CH_4) to the feed gas did not significantly alter the results.

5. Preliminary tests showed that it is possible, under some conditions, to reverse degradation in the performance of ANL-3e membranes that is caused by exposure to H_2S.

6. Several methods were developed to fabricate hydrogen transport membrane (HTM) and oxygen transport membrane (OTM) thin films on porous substrates.

7. High-pressure hydrogen permeability measurements at NETL suggest that concentration polarization might influence the hydrogen flux under some conditions.

8. Hydrogen flux measurements indicate that ANL-3e membranes are stable in feed gas with up to 0.49 atm H_2O at temperature up to 900°C.

III. INTRODUCTION

This goal of this project is to develop two types of dense ceramic membrane for producing hydrogen nongalvanically, i.e., without electrodes or external power supply, at commercially significant fluxes under industrially relevant operating conditions. The first type of membrane, hydrogen transport membranes (HTMs), will be used to separate hydrogen from gas mixtures such as the product streams from coal gasification, methane partial oxidation, and water-gas shift reactions. Potential ancillary uses of HTMs include dehydrogenation and olefin production, as well as hydrogen recovery in petroleum refineries and ammonia synthesis plants, the largest current users of deliberately produced hydrogen. The second type of membrane, oxygen transport membranes (OTMs), will produce hydrogen by nongalvanically removing oxygen that is generated when water dissociates at elevated temperatures. This report describes progress that was made during FY 2006 on the development of OTM and HTM materials.

Materials development for the HTM follows a three-pronged approach. In one approach, we utilize principles of solid-state defect chemistry to properly dope selected monolithic electronic/protonic conductors (perovskites doped on both A- and B-sites) and thereby obtain materials that are chemically stable and have suitable protonic and electronic conductivities. Hydrogen transport through such materials is maximized when the protonic and electronic conductivities are high and nearly equivalent. Cermet (i.e., ceramic/metal composite) membranes are the focus of our second approach, in which mixed electronic/protonic conducting ceramics are intimately mixed with a metallic component. The metal phase in these cermets enhances the hydrogen permeability of the ceramic phase by increasing the electronic conductivity, and can provide an additional transport path for the hydrogen if the metal has high hydrogen permeability. In our third approach, we disperse a hydrogen transport metal, i.e., metal with high hydrogen permeability, in a support matrix composed of either a ceramic or a metal. In these composites, hydrogen is transported almost exclusively through the hydrogen transport metal, and the matrix serves primarily as a chemically stable structural support. The properties of OTMs are similarly manipulated either by appropriately doping a mixed electron/oxygen ion conductor or incorporating it in a cermet membrane.

Table 1 summarizes the compositions of membranes that have been developed to date at Argonne. The membranes are classified as ANL-1, -2, or -3, based on the transport properties of their metal and ceramic phases; e,g., ANL-1a and –2a membranes are HTMs that contain a mixed electronic/protonic conductor and produce hydrogen via hydrogen permeation from the feed gas, whereas ANL-1b, -1c, and -2b membranes are OTMs that contain a mixed electron/oxygen ion conductor and produce hydrogen through water splitting. An ANL-1 membrane contains a metal with low hydrogen permeability, whereas an ANL-2 membrane contains a hydrogen transport metal. ANL-3 membranes contain a hydrogen transport metal that is dispersed in a ceramic matrix with

low hydrogen permeability, e.g., Al_2O_3, ZrO_2, or $BaTiO_3$. To date, thin film ANL-3e membranes have given the highest hydrogen flux [≈22 cm^3(STP)/min-cm^2 at 500°C and ≈32 cm^3(STP)/min-cm^2 at 900°C] for Argonne membranes. In this classification scheme, the letter following a number in a membrane's designation indicates a particular combination of metal and matrix phases, e.g., ANL-3a membranes contain "metal-a" in a matrix of Al_2O_3, whereas ANL-3b membranes contain a different metal and/or a different ceramic matrix.

Table 1. Compositions of Argonne Membranes

Membrane	Type	Matrix	Metal
ANL-0	HTM	BCY	----
ANL-0b	OTM	SFC2	----
ANL-0c	OTM	SFT1	----
ANL-1a	HTM	BCY	Ni
ANL-1b	OTM	CMO	Ni
ANL-1c	OTM	TZ-8Y	Ni
ANL-1d	OTM	SFT1	Ni
ANL-2a	HTM	BCY	Pd
ANL-2b	HTM/OTM	CMO	Pd/Ag(23 wt.%)
ANL-3a	HTM	Al_2O_3	Pd
ANL-3b	HTM	$BaTiO_3$	Pd/Ag
ANL-3c	HTM	Al_2O_3	Nb
ANL-3d	HTM	Al_2O_3	Pd/Ag(23 wt.%)
ANL-3e	HTM	TZ-3Y	Pd
ANL-3f	HTM	TZ-8Y	Pd
ANL-3g	HTM	$CaZrO_3$	Pd
ANL-4a	HTM	Cu	Nb

Notes: BCY = $BaCe_{0.8}Y_{0.2}O_{3-\delta}$, CMO = $Ce_{1-x}M_xO_{2-\delta}$(M: Gd, Y),
TZ-3Y = ZrO_2 (3 mol.% Y_2O_3), TZ-8Y = ZrO_2 (8 mol.% Y_2O_3),
SFC2 = $Sr_{1.0}Fe_{1.0}Co_{0.5}O_x$, SFT1 = $Sr_{1.0}Fe_{0.9}Ti_{0.1}O_x$

Good chemical stability is a critical requirement for HTMs that Argonne is developing for separating hydrogen from the product streams of coal gasification and/or methane reforming processes. Because HTMs will encounter hydrogen sulfide (H_2S), which degrades Pd-containing HTMs by forming palladium sulfide (Pd_4S), we are testing

ANL-3e membranes to determine the conditions under which Pd_4S forms. Tests [1] showed that, in feed gas of 73% H_2/400 ppm H_2S/balance He, the Pd/Pd_4S phase boundary lies at 600-650°C. Extending our study of the Pd/Pd_4S phase boundary in this report, we show results from tests using feed gases of 73% H_2/≈190 ppm H_2S/balance He and 73% H_2/≈60 ppm H_2S/balance He. We report the Pd/Pd_4S phase boundary in feed gas containing 73% H_2/0.497% CH_4/6.188% CO_2/7.8455% CO/400 ppm H_2S/balance He to begin assessing the effect of syngas components on the Pd/Pd_4S phase boundary, and we evaluate the chemical stability of an ANL-3e membrane in the presence of steam by measuring its hydrogen flux in feed gas that contained 0.03-0.49 atm H_2O.

In addition to chemical stability in corrosive environments, HTMs must have good mechanical integrity at high temperature (≈900°C) and high pressure (≈350 psi). To judge the performance of Argonne membranes at high pressures, multiple tests have been conducted in the high-pressure test facility at the National Energy Technology Laboratory (NETL). Although commercial compression fittings have been used to successfully seal membranes for tests at NETL, three compression seals made at Argonne began leaking during the initial heat-up at NETL even though preliminary tests at Argonne were "successful", i.e., showed no leakage at room temperature under a pressure of 35 psig helium. The development of leaks during heat-up after successful tests at Argonne showed that low-pressure testing at room temperature gives little information about the performance of seals at high temperatures and high pressures. To aid further development of gas-tight seals and provide high-pressure testing of Argonne membranes, we constructed a reactor that allows membranes and seals to be tested at temperature up to 900°C and pressure up to 300 psig. The first flux measurements made with Argonne's high-pressure reactor are presented in this report.

The following milestones were established in the Field Work Proposal for FY 2006:

1. Test membrane stability in coal gasifier-like gases at temperatures ≤600°C.
2. Test membrane in high-pressure feed streams at Argonne.
3. Perform integrated gasification combined-cycle (IGCC) analysis for membranes at 900°C.
4. Determine Pd/Pd_4S phase boundary.

All milestones for FY 2006 were met using membranes that were developed at Argonne. In addition to meeting the milestones, we continued developing new membrane materials and fabrication methods in order to enhance the hydrogen flux of HTMs and the hydrogen production rate of OTMs.

IV. RESULTS

Results obtained during FY 2006 are presented below in relation to the pertinent milestone. After discussing the work related to the milestones, results obtained outside the scope of the milestones are described.

Milestone 1. Test membrane stability in coal gasifier-like gases at temperatures ≤600°C.

Feed gases containing ≤400 ppm H_2S were prepared to simulate coal gasifier-like gases. The powder mixture used to make ANL-3e membranes for testing chemical stability and measuring hydrogen flux was prepared by mixing Pd (50 vol.%) powder with TZ-3Y (i.e., ZrO_2 partially stabilized with Y_2O_3) powder from Tosoh Ceramics. The Pd/TZ-3Y mixture was uniaxially pressed into disks that were sintered at 1400-1500°C for 5-10 h in ambient air. Because hydrogen flux was measured for relatively short periods (<200 h), the sample was sealed using simple gold rings rather than wrapping gold around its edges, as has been done in long-term tests [2]. The initial flux (time=0 h) was measured using 73% H_2/balance He (with no H_2S) as the feed gas, after which the feed gas was switched to 73% H_2/400 ppm H_2S/balance He. Gas mixtures were prepared using mass flow controllers (MKS 1179A) to blend appropriate amounts of three gases: He, H_2, and either 1100 ppm H_2S/balance H_2 or 1240 ppm H_2S/balance H_2. The flow rate of gas mixtures was 200 cm^3/min and the sample chamber had a volume of ≈2600 cm^3; therefore, a volume of gas equivalent to the volume of the sample chamber flowed into the chamber in ≈13 min, and the composition of gas in the sample chamber is expected to equal the feed gas composition within ≈1 h after changing the feed gas composition.

Membrane microstructures and thickness were examined using a JEOL 5400 scanning electron microscope (SEM). Energy dispersive spectroscopy (EDS) for chemical analysis of microstructural features was done using a Voyager system from Thermo Electron Scientific Instruments Corp. To prepare sintered disks for hydrogen flux measurements, both sides were polished using 600-grit SiC polishing paper. The ANL-3e membrane for the test at 600°C had a thickness of ≈240 μm; the membrane tested at 500°C had a thickness of ≈230 μm. The procedures for measuring hydrogen flux are described elsewhere [3]. For a given condition, the hydrogen and helium concentrations in the sweep stream were measured 2-4 times using a gas chromatograph (SRI 8610C), and the average of those readings were used to calculate the hydrogen flux. Individual readings varied from the average value by ≤10%. The values of hydrogen flux were corrected for leakage based on the measured helium leakage rate.

Figure 1 plots hydrogen flux versus time for two ANL-3e membranes that were tested using 73%H_2/400 ppm H_2S/balance He as feed gas. One membrane was tested at 500°C, and the other was tested at 600°C. The thickness of each membrane is given in the legend of Fig. 1. Each experiment began by measuring the flux using a feed gas of 73%H_2/balance He (no H_2S) and then switching to H_2S-containing gas at time t=0 h. The error bars in Fig. 1 indicate ±10% of the reported flux value.

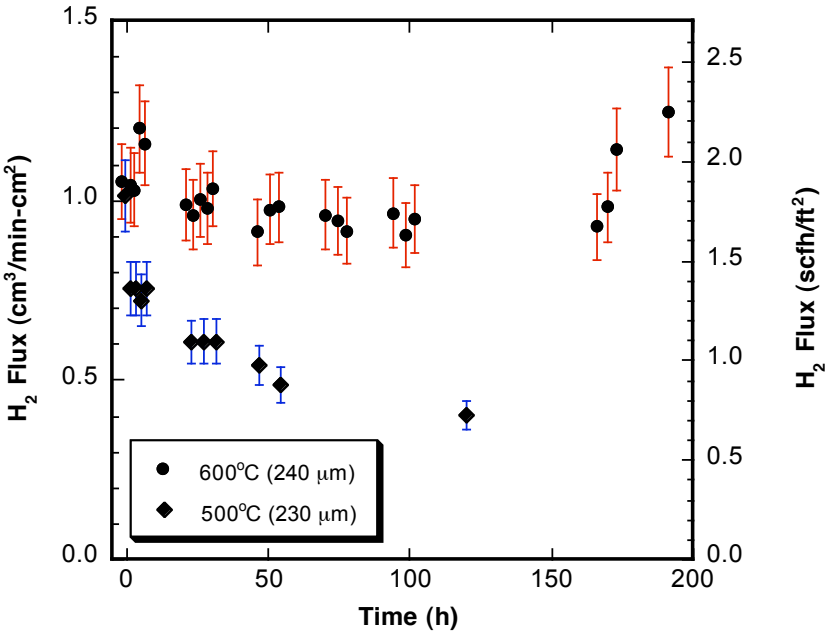

Fig. 1 H_2 flux for two ANL-3e membranes, one tested at 500°C, one at 600°C, using 73% H_2/400 ppm H_2S/balance He as feed gas. Inset gives membrane thickness for each experiment.

The flux at 600°C increased soon (≈4.5 h) after gas containing 400 ppm H_2S began flowing. The increase is anomalous, because the flux immediately decreased again and stabilized at a value that was only ≈10% lower than its initial value. A decrease of ≈10% is typical of stability studies that were conducted at higher temperatures. After monitoring the flux for ≈170 h, the feed gas was switched back to 73% H_2/balance He (no H_2S), and the flux increased. After leaving the sample overnight in 73% H_2/balance He at 600°C, the flux was slightly higher than its original value. The increase in flux suggested that ANL-3 membranes might be regenerated after they have reacted with H_2S-containing gases. This possibility was studied further, as described later in the section on additional results. After exposing the sample overnight to 73% H_2/balance He (no H_2S), the feed gas was switched to helium, and the sample was cooled to room temperature.

The flux decreased more rapidly and by a larger total amount (Fig. 1) when the sample was exposed to 73% H_2/400 ppm H_2S/balance He at 500°C. After ≈120 h, the flux had dropped by ≈50%, and it appeared that the flux had not stabilized. No attempt was made to "regenerate" this sample by heating it in hydrogen-containing gas without H_2S; it was simply cooled to room temperature in flowing helium.

A reaction layer was evident on the feed surface of both membranes after the flux measurements at 500 and 600°C. SEM/EDS showed an ≈10 μm-thick layer of Pd_4S on the feed surface of the sample tested at 500°C (Fig. 2a), suggesting that Pd_4S had caused the sample's flux to decrease. A uniform layer also covered the feed surface of the sample tested at 600°C (Fig. 2b), but the layer was thinner and its composition was pure Pd. It was presumed that Pd_4S had formed during the exposure to H_2S at 600°C but later decomposed when 73% H_2/balance He (no H_2S) flowed over the sample. This idea was

consistent with the increase in flux at 600°C when the feed gas was switched overnight to 73% H_2/balance He (no H_2S), and it was supported by our subsequent study indicating that an ANL-3e membrane can be regenerated after it reacts with H_2S. To better understand the effects of H_2S on Pd-containing ANL-3 membranes, the Pd/Pd_4S phase boundary was studied in more detail. Results from that study are given below in the section about the milestone for the fourth quarter.

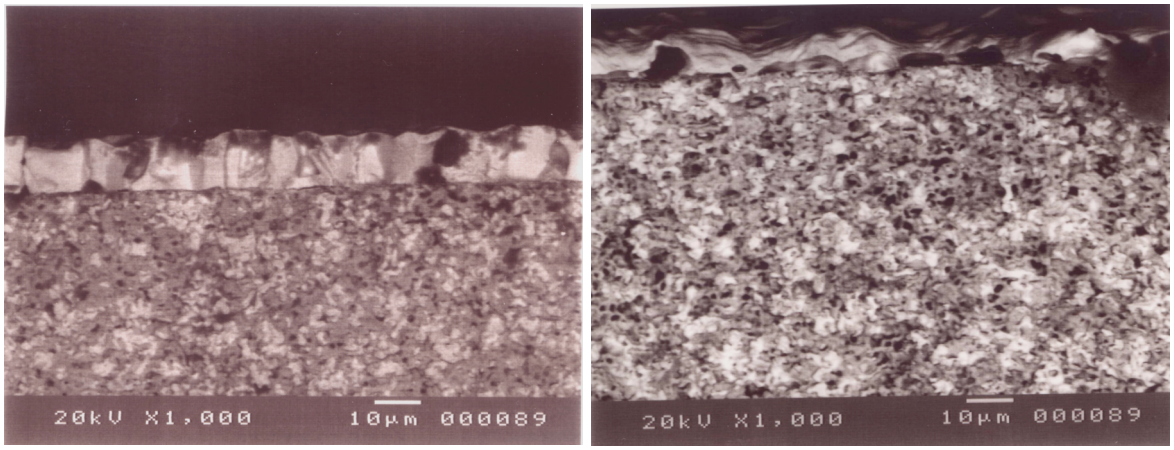

(a) (b)

Fig. 2 Cross-sectional views of ANL-3e membranes after flux measurements using 73% H_2/400 ppm H_2S/balance He as feed gas at a) 500 and b) 600°C. Light-shaded areas are Pd or Pd_4S; dark areas are partially stabilized ZrO_2.

Milestone 2. Test membrane in high-pressure feed streams at Argonne.

In addition to being chemically stable in corrosive environments, HTMs must give a high hydrogen flux and have good mechanical integrity at high temperature (≈900°C) and high pressure (≈350 psi). To judge the performance of Argonne membranes at high pressures, multiple tests have been conducted in the high-pressure test facility at NETL. Although commercial compression fittings have been used to successfully seal membranes for some of the tests, three compression seals made at Argonne leaked during the initial heat-up at NETL even though preliminary tests at Argonne were "successful", i.e., showed no leakage at room temperature under a pressure of 35 psig helium. The development of leaks during heat-up after successful tests at Argonne showed that low-pressure testing at room temperature gives little information about the performance of seals at high temperatures and high pressures. To aid the development of gas-tight seals and accelerate high-pressure testing of Argonne membranes, we constructed a reactor that allows membranes and seals to be tested at temperature up to 900°C and pressure up to 300 psig. We describe here the initial flux measurements that were obtained with Argonne's high-pressure reactor, shown in Fig. 3.

The reactor sits inside a ventilation hood in order to capture hydrogen that could leak from the reactor if a sample or a seal fails. Leakage from the reactor is minimized by

enclosing the sample/seals in a secondary containment tube that is constantly purged by inert gas (100 ppm H_2/balance N_2) flowing into the building exhaust. Figure 4 shows that the sample is sealed between two tubes made of Haynes HR-160, a high-strength alloy with a maximum allowable stress of 1300 psi at 1650°F (899°C) [4]. During testing, feed gas (≤300 psig H_2) flows through a tube and then over one side of the sample, while sweep gas (≤300 psig N_2) flows through another tube and over the other side of the sample. Both gases are vented to building exhaust after they flow over the sample. The flow rates of the feed and sweep gases can be varied from 50-1000 ml/min. Hydrogen and helium concentrations in the sweep gas are measured by briefly (≈45 s) diverting the sweep gas from building exhaust to a gas chromatograph (GC).

Fig. 3 Argonne's hydrogen permeation reactor rated to operate at up to 900°C and 300 psig.

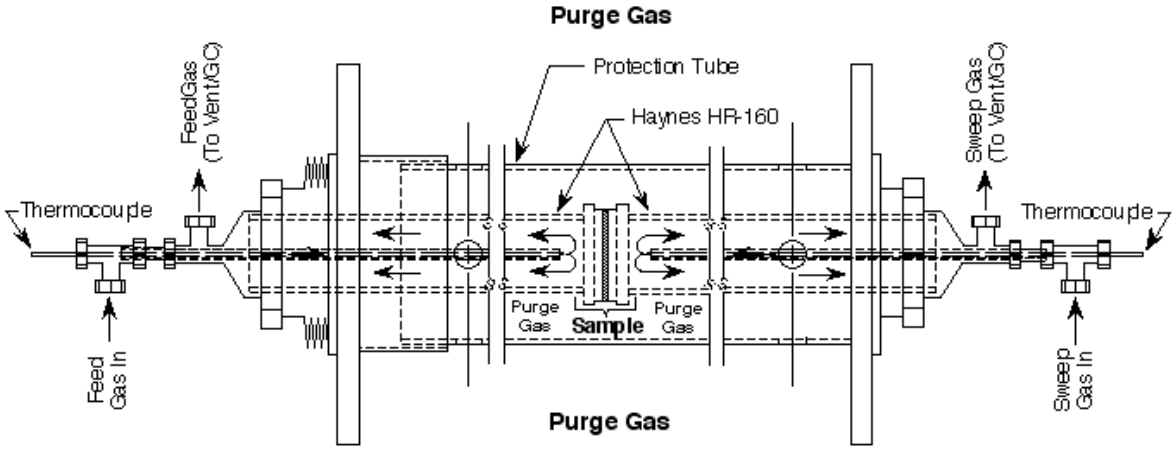

Fig. 4 Gas flow patterns in furnace for Argonne's 900°C/300 psig H_2 permeation reactor.

Figure 5 shows that the sample (4) and high-pressure HR-160 tubes (2) are placed inside protection tube (3), which is inside a cylindrical heating element (19), all of which is contained in a secondary containment tube (13). The protection tube protects the heating element from gas that would flow at high velocity in the event of a leak from the sample, seals, or HR-160 tubes; it also protects the heating element when the sample and tubes are loaded into the reactor. The protection tube is welded to endcap (10) on the right of the reactor, and slides into sleeve (5), which is welded to the reactor's left endcap (10). Because the protection tube slides freely into the sleeve and does not extend all the way to the left endcap, it expands freely when the reactor is heated. Holes (11) in the protection tube allow gas to escape into the purge chamber in the event of a gas leak. The endcaps are sealed onto the secondary containment tube (13) using threaded rods (26) to pull the endcaps together and squeeze rubber gaskets (27) between the endcaps and the secondary containment tube.

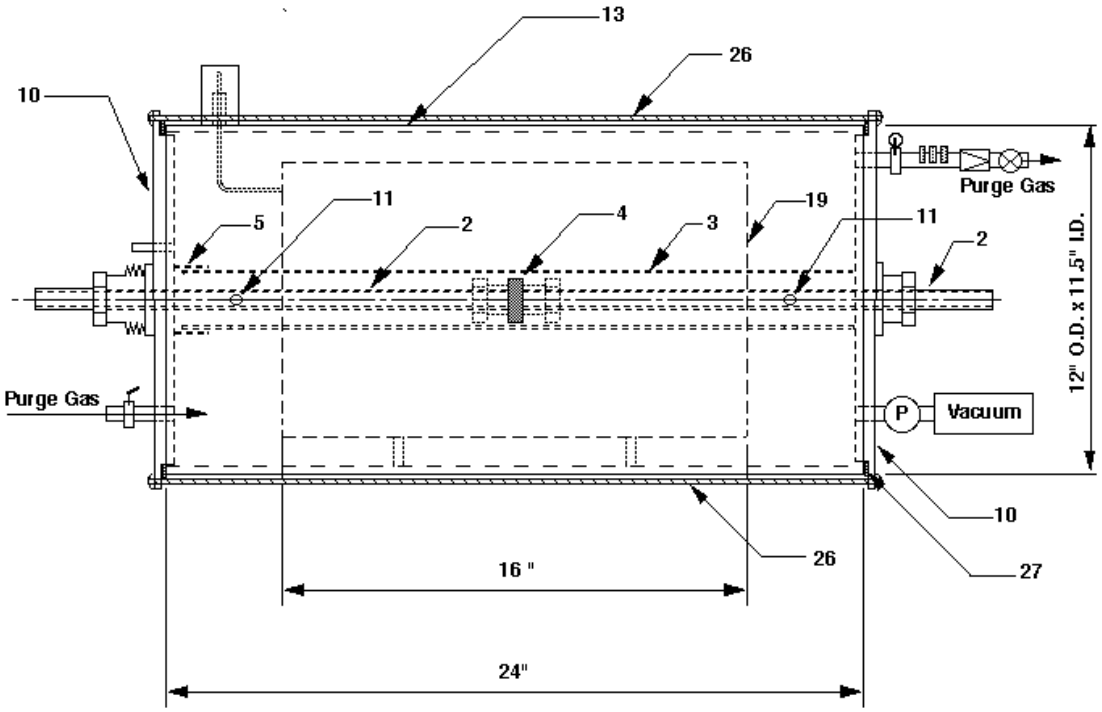

Fig. 5 Furnace for Argonne's new 900°C/300 psig H_2 permeation reactor.

Figure 6 shows an overview of the reactor system. Backpressure regulators (38) control pressure on the feed and sweep sides of the sample. Mass flow controllers (35) control the flow rates of feed and sweep gases into the reactor, while mass flow meters (33) measure the flow rates of feed and sweep gases out of the reactor. A purge gas composed of 100 ppm H_2/balance N_2 flows through the secondary containment tube (13) to carry leakage from the reactor to the building exhaust. Sensors (15), (16), and (17) monitor the purge gas as it exits the reactor, and a pneumatic valve stops the flow of feed and sweep gases if any of the following alarm conditions occurs:

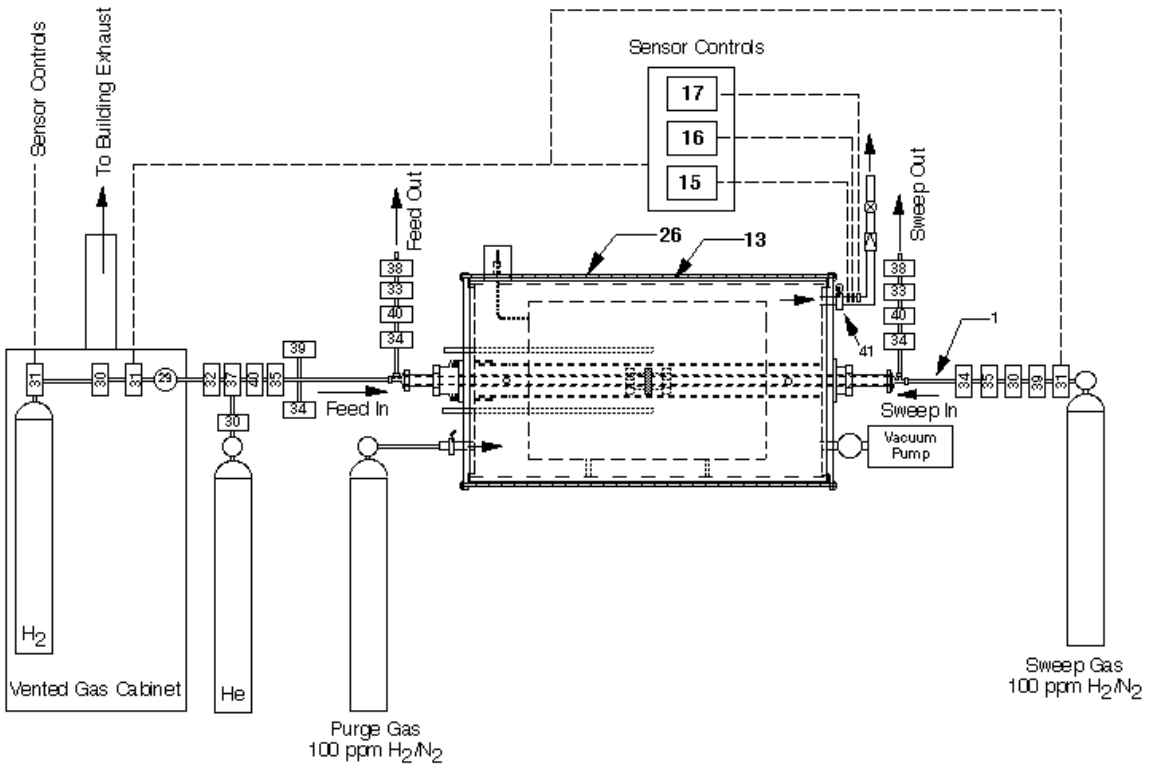

Fig. 6 Argonne's 900°C/300 psig H_2 permeation reactor system.

Alarm 1: H_2 sensor (15) detects a H_2 concentration $\geq\approx 1\%$ (i.e., >25% of the Lower Explosive Limit), which would indicate that sample/seal (4) or tubes (2) are leaking,

Alarm 2: O_2 sensor (16) measures >2% O_2, which would indicate that ambient air had not been completely removed from the purge chamber or was leaking into the chamber. Hydrogen atmospheres containing <4 vol.% O_2 are reported to be inert [5].

Alarm 3: Pressure transducer (17) indicates the pressure inside the purge chamber is <0.7 psig, a pressure that is maintained to prevent ambient air from leaking into the purge chamber.

Alarm 4: The flow rate of feed (or sweep) gas into the reactor differs from the flow rate of that gas out of the reactor by ≥50 ml/min. If there are no leaks in the high-pressure part of the system, the flow rates into the reactor will equal the flow rates out of the reactor (taking into account that the flow rate of feed gas out of the reactor will be less than the feed flow rate into the reactor by the amount of H_2 that permeates through the sample and HR-160 tubes). A significant difference between the flow rate into the reactor and the flow rate out of the reactor would indicate a leak in the high-pressure system.

Alarm 5: The pressure of either the feed gas or the sweep gas exceeds 325 psig. This release pressure allows the reactor to be operated at its maximum operating pressure

(300 psig) without closely approaching the maximum allowable pressure (392 psig) that was calculated using the ASME Boiler Code [4].

Alarm 6: The linear air velocity into the exhaust ductwork falls below 50 ft/min, which is ≈six times larger than the air velocity necessary to ensure that the gas in the exhaust duct does not exceed the lower explosive limit.

Figures 5 and 6 show the locations of additional safety devices. The inlet sides for the feed and sweep gases are protected by pressure relief valves (39) and excess flow valves (30). The pressure relief valves were preset at the factory to release at 350 psig. The pressure relief valves provide redundant control of the feed/sweep pressure in addition to the pressure transducers used to set off Alarm 5 described above. A pressure relief valve, set to release at 5 psig, prevents the purge chamber from being over-pressurized. Excess flow valves were preset at the factory to shut off the flow of gas if the flow rate exceeds 3 liters/min. A flashback arrestor also protects the feed side inlet. A check valve prevents ambient air from diffusing into the purge chamber from the exhaust line. Another H_2 sensor, not shown in the figures, is positioned outside the hood for the reactor and will shut down the flow of gases to the high-pressure reactor and all other reactors if the H_2 concentration in the room exceeds 2% H_2 (50% LEL).

The hydrogen flux of an ANL-3e membrane (thickness ≈0.91 mm) was measured in the high-pressure reactor at temperatures up to 900°C and total pressures up to 280 psig. Both sides of the sample were polished using 600-grit SiC polishing paper, and the sample was sealed between two high-strength Haynes HR-160 tubes using graphite gaskets in a VCR-type fitting. The feed gas composition was 3.78% H_2/balance He, and the sweep gas composition was 100 ppm H_2/balance He. After establishing selected total pressures in the feed and sweep streams, the flux was measured at ≈100°C-increments in the range 500-900°C. The pressures in the feed and sweep streams were then changed, and the flux was measured again over the range 500-900°C. The total pressure in the feed and sweep streams was varied in ≈50 psi-increments up to a maximum of 280 psig. For each total pressure that was established, the total pressures in the feed and sweep streams differed by <5 psi. For each combination of temperature and total pressure, the hydrogen and helium concentrations in the sweep stream were measured at least four times using a Hewlett-Packard 6890 GC. To calculate the hydrogen flux, the hydrogen concentration in the sweep stream was corrected for leakage (based on the measured helium leakage rate) and for the H_2 concentration (100 ppm) that was initially present in the sweep stream.

Figure 7 plots hydrogen flux values that were measured in the high-pressure permeation reactor versus $\Delta pH_2^{1/2}$, a quantity that is given in terms of the partial pressures of hydrogen on the feed and sweep sides of the membrane:

$$\Delta pH_2^{1/2} \equiv \sqrt{pH_2(\text{feed})} - \sqrt{pH_2(\text{sweep})}\,.$$

At each temperature, the flux varies linearly with $\Delta pH_2^{1/2}$, as expected for hydrogen diffusion through a metal. As temperature increases, the slope increases due to the increase in the membrane's hydrogen permeability. Although the flux measurements were

made using total pressure in the feed gas up to ≈280 psig, the maximum value of $\Delta pH_2^{1/2}$ reached only ≈0.7 $atm^{1/2}$ because the hydrogen concentration in the feed gas (3.78% H_2) was restricted to nonflammable values during this experiment due to safety considerations. This was necessary, because it was discovered during the initial heat-up that the hydrogen sensor was not functioning properly. When the hydrogen sensor functions properly, hydrogen flux will be measured at values of $\Delta pH_2^{1/2}$ up to ≈3.5 $atm^{1/2}$.

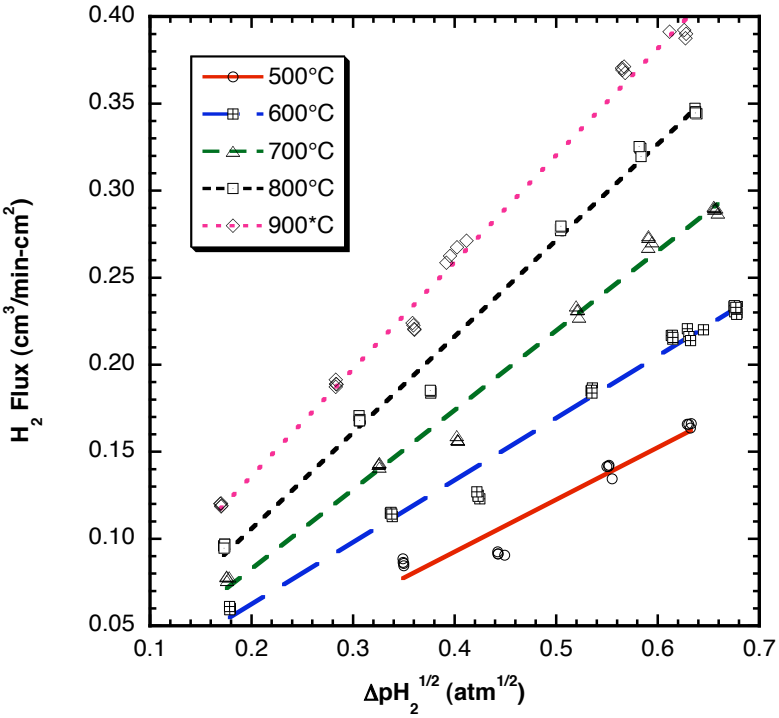

Fig. 7 Hydrogen flux for 0.91-mm-thick ANL-3e membrane measured in Argonne's new high-pressure permeation reactor. Feed gas had composition of 3.78% H_2/balance He and total pressure up to ≈280 psig.

Figure 8 compares hydrogen flux values measured in our high-pressure reactor to values that were measured [2] at Argonne in an ambient-pressure reactor and at NETL using their high-pressure facility [2]. In the ambient-pressure reactor, $\Delta pH_2^{1/2}$ was varied by changing the composition of the feed gas while maintaining a total pressure of 1 atm, whereas $\Delta pH_2^{1/2}$ was varied in Argonne's high-pressure reactor by changing the total pressure while the composition of feed gas was fixed at 3.78% H_2/balance He. To plot the data in Fig. 8, all flux values measured in the high-pressure reactor were normalized for a thickness of ≈20 mm. The straight lines show linear fits of the data measured at ambient pressure and are provided mainly as guides to the eye. The values measured in Argonne's high-pressure reactor are consistent with the values that were measured previously at ambient pressure and at high-pressure at NETL, suggesting that the values obtained using Argonne's high-pressure reactor are reasonable.

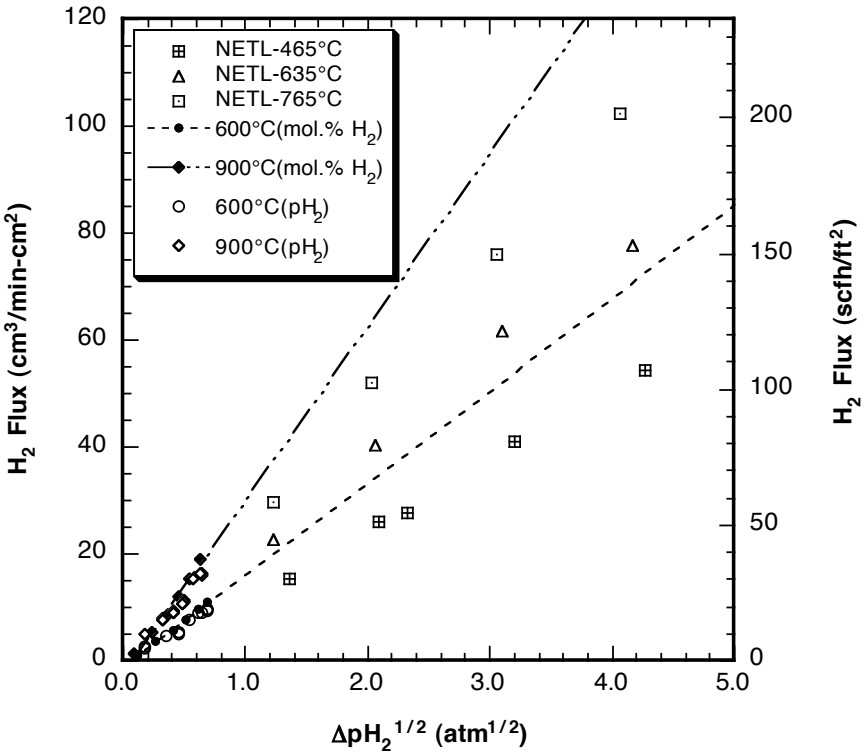

Fig. 8 H_2 flux of ANL-3 membranes, measured by varying pH_2 in Argonne's high-pressure reactor and NETL's high-pressure facility [2] and by varying mol.% H_2 in Argonne's ambient-pressure reactor [2].

Milestone 3. Perform integrated gasification combined-cycle (IGCC) analysis for membranes at 900°C.

Integrating process design aids the development of an economical IGCC hydrogen production system that uses HTMs by focusing the development efforts on those areas that directly impede commercialization. In addition to identifying novel equipment, estimating its cost, and considering challenges with interfacing the equipment with the overall system, we will explore opportunities to optimize the overall process. Considerations of particular interest include the heat source temperature, pressure and duty requirements, the heat carrier medium, and the conditions and purity of the process streams. These considerations will be incorporated into the IGCC design using the Aspen Plus® Simulation module which has been previously employed for NETL to study both the Texaco and Shell gasifiers as conversion routes to hydrogen.

Early industrial-scale chemical processes were scaled up from laboratory experiments using largely empirical designs. As experience with these industrial-scale processes was gained, however, similarities in the necessary process equipment were recognized, and analytical and heuristic methods were developed to design commonly used types of equipment. Because membrane technology represents a departure from the common types of equipment, we will need to develop user modules for membrane units, while keeping the balance of the plant based on well-understood equipment.

ASPEN process modeling assumes known performance of reactors, separators, purifiers, and power equipment. For this effort, we characterize multi-component input and output streams using physical properties programs valid at operating temperatures and pressures while ASPEN calculates intermediate flows, energy requirements, and residuals.

Carbon dioxide (CO_2)-capture technologies, combined with Shell integrated gasification combined-cycle (IGCC) power systems that produce both merchant hydrogen (H_2) and electricity, could operate on either low- or high-sulfur coals. An oxygen-blown entrained gasifier served as the basis for the study. Comparisons of energy penalties, capital investment, and CO_2-emission reductions were based on the full energy cycle—including mining, coal transportation, coal preparation, gasification, gas treatment, power generation, infrastructure to transfer power or hydrogen to end users, and pipeline transport of CO_2 for sequestration. Figure 9 shows the base case configuration for the system, which has slight modifications that recycle SCOT gases to the gasifier. This work was reported previously [6].

The same gasifier model [Shell IGCC Base Sb50b10 obtained from Wally Shelton (NETL) and reported in PED-IGCC-98-002, using 3,000 tons/day of high-sulfur Illinois #6 coal] was used to evaluate the utilization of HTMs. For the base case (generating only electric power without CO_2-recovery), the system delivers 450 MW gross/400 MW net electricity. The Texaco gasifier TX-QU120 model, obtained from Wally Shelton (NETL) and tested during this period, could also be employed to evaluate the effects of HTMs.

Modifications to the base case layout appear in Fig. 10. In the base case (Fig. 9), raw gas from the Shell gasifier (2500°F) is quenched to 1850°F with a recycle stream of cooled raw gas, and is then used to raise steam. Rather than lose heat in such a quench, the HTM-modified process (Fig. 10) uses the high-temperature (2500°F) raw gas to heat the HTMs and produce hydrogen from the high-H_2S 1st stage shift product. Various heat exchange configurations could prove workable for this service and are being considered. In the HTM-modified approach, the second stage of shift is eliminated, and a portion of the gas continues downstream as fuel gas for the turbine HRSG and for clean-up and recovery of CO_2.

An ASPEN base case for the hydrogen separation membranes will be run for the 900°C (1650°F) case exchanging against the raw gas that currently is being quenched. A ceramic heat exchanger for gas-gas service on gasifier raw-gas cooling will be used prior to quench to drive the ceramic membranes (2500-1850°F; 450 psi). This should improve process efficiency.

While the second stage of shift will be eliminated by the approach shown in Fig. 10, the optimal split needs to be considered and then used to set the portion of the gas that will continue downstream for clean-up and recovery of CO_2 and to provide fuel gas to the turbine HRSG. Possibly a final stage of product H_2 recovery in PSA may be used if it is cost effective.

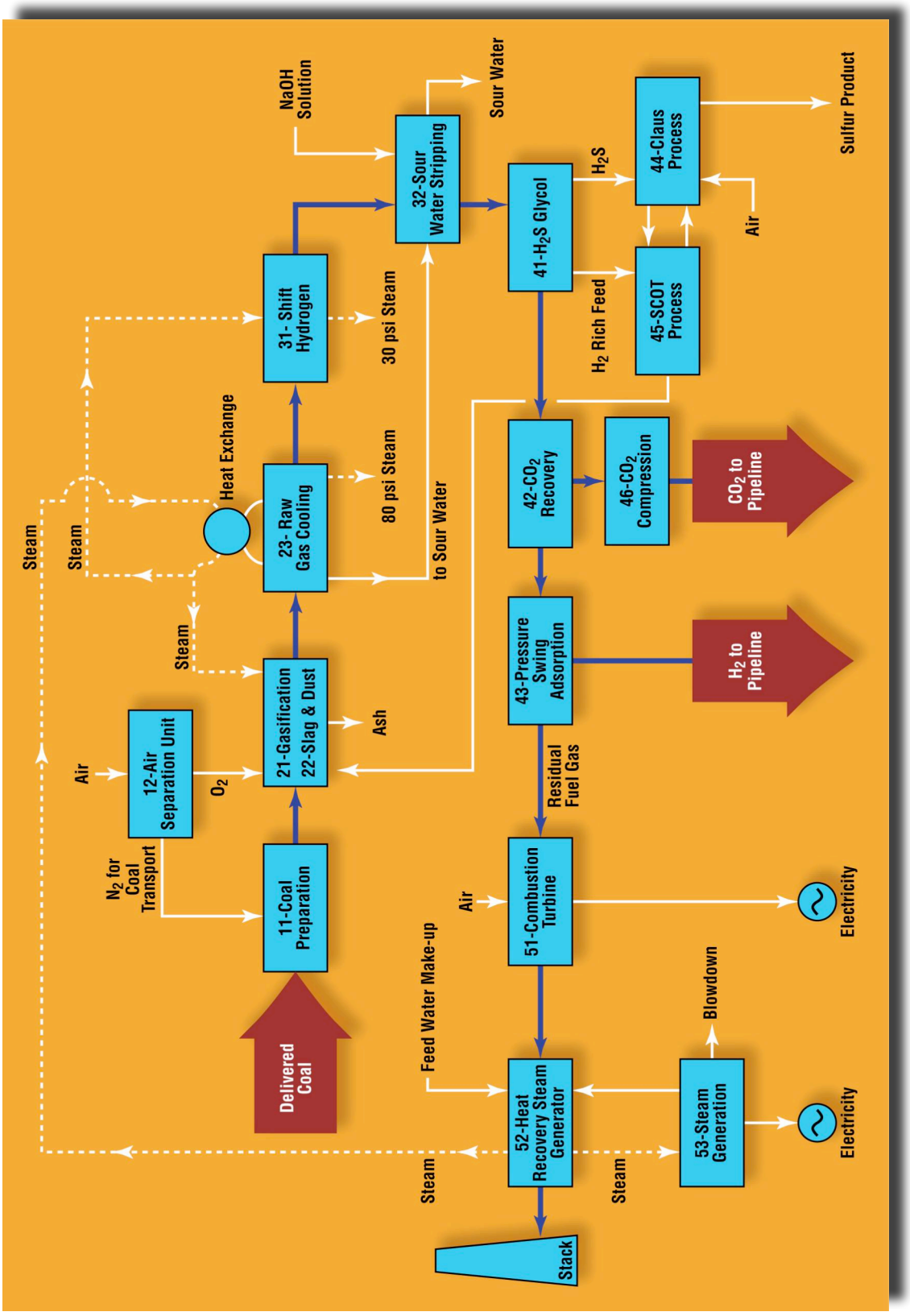

Fig. 9 Schematic for Shell IGCC with Illinois #6 coal. Base case for H_2 production.

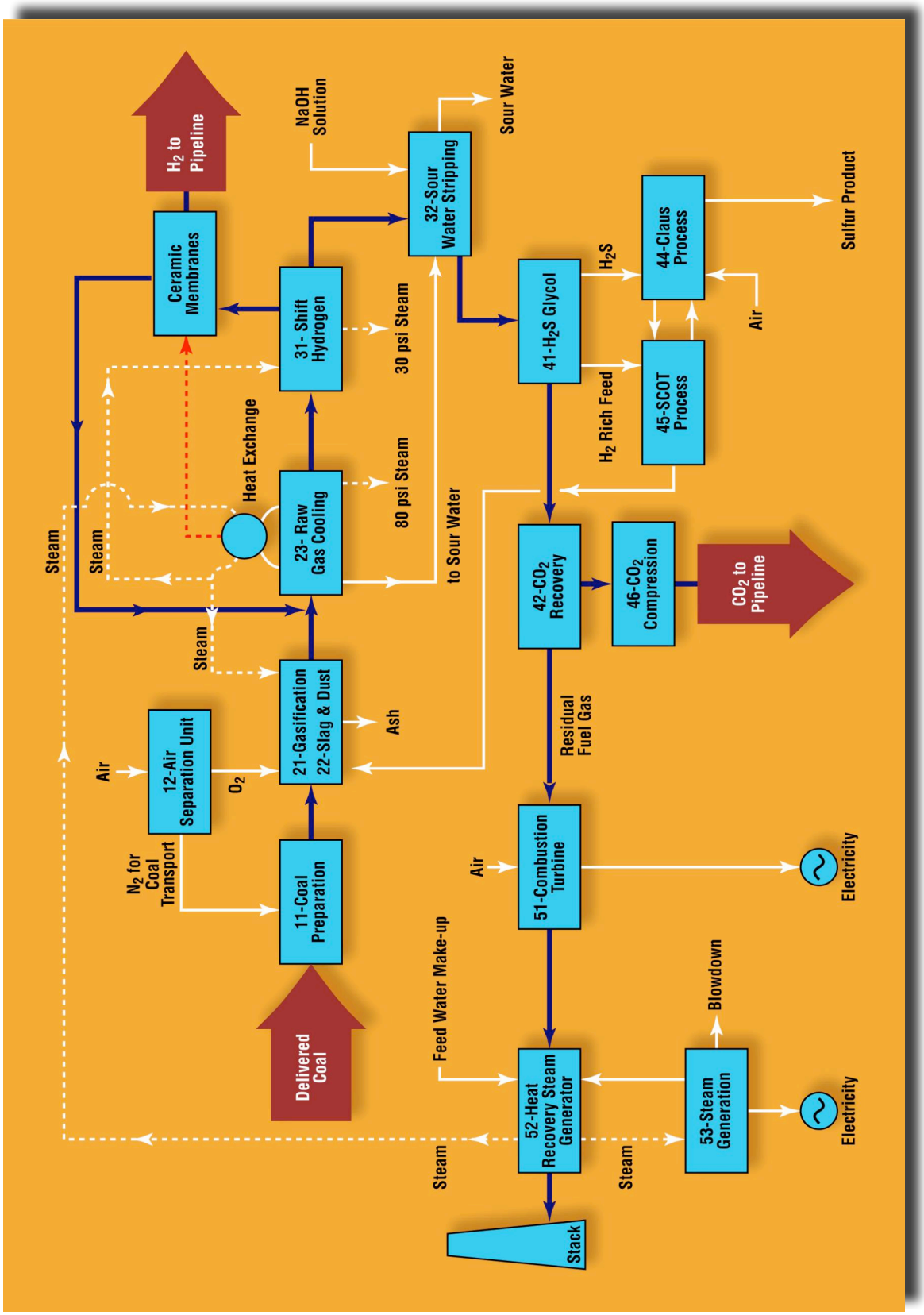

Fig. 10 Schematic for Shell IGCC with Illinois #6 coal - H_2 production using HTM.

Milestone 4. Determine Pd/Pd_4S phase boundary.

Chemical stability is a critical requirement for HTMs that will separate hydrogen from the product streams of coal gasification and/or methane reforming processes. Because HTMs will encounter hydrogen sulfide (H_2S), which degrades Pd-containing HTMs by forming palladium sulfide (Pd_4S), we are identifying conditions under which Pd_4S forms by determining the position of the Pd/Pd_4S phase boundary. Using ANL-3e membranes, we are locating the phase boundary in feed gases containing various concentrations of H_2 and H_2S, and are assessing the effect of syngas components on the phase boundary's location. Because the H_2 concentration affects the position of the phase boundary, the H_2 concentration has been held constant (≈73% H_2) in all experiments done to this point.

The powder mixture for making ANL-3e samples was prepared by mixing TZ-3Y (i.e., ZrO_2 partially stabilized with Y_2O_3) powder from Tosoh Ceramics with Pd powder (50 vol.%) from Technic, Inc. ANL-3e samples were prepared by uniaxially pressing the Pd/TZ-3Y powder mixture into disks (≈5 mm dia.) and then sintering them for 5-10 h in ambient air at 1400-1500°C.

Gas mixtures were prepared using mass flow controllers (MKS 1179A) to blend the gases listed in Table 2. The flow rate of the gas mixture was 200 cm^3/min during the equilibration, and the sample chamber had a volume of ≈2600 cm^3. Therefore, a volume of gas equivalent to the chamber volume flowed into the chamber in ≈13 min, and the gas composition in the sample chamber could be expected to equal the feed gas composition within ≈1 h after changing the feed gas composition.

Table 2. Composition of gases used to determine Pd/Pd_4S phase boundary.

Feed Gas Composition	Gases used to prepare Mixture
73% H_2/60 ppm H_2S/balance He	Pre-mixed by Linde
73% H_2/190 ppm H_2S/balance He	Pre-mixed by Linde
73% H_2/400 ppm H_2S/balance He	H_2 0.124% H_2S/balance H_2 He
73% H_2/400 ppm H_2S + 6.3% CH_4/6.8% CO_2/8.8% CO/balance He **Discontinued due to coke formation**	10% CH_4/11% CO_2/14% CO/balance H_2 0.124% H_2S/balance H_2 He
73% H_2/60 ppm H_2S + 0.2% CH_4/2.8% CO_2/3.5% CO/balance He	1% CH_4/11% CO_2/14% CO/balance H_2 500 ppm H_2S/balance H_2 He
73% H_2/200 ppm H_2S + 0.4% CH_4/5.0% CO_2/6.4% CO/balance He	1% CH_4/11% CO_2/14% CO/balance H_2 108 ppm H_2S/balance H_2 He
73% H_2/400 ppm H_2S + 0.5% CH_4/6.2% CO_2/7.8% CO/balance He	1% CH_4/11% CO_2/14% CO/balance H_2 0.124% H_2S/balance H_2 He

Equilibrations were done by heating a sample at a rate of 180°C/h in flowing He, and then switching to one of the feed gas mixtures listed in Table 2 when the selected temperature was reached. After holding the sample at that temperature for 24 h, the feed gas was switched back to He. The sample was held at that temperature for 6 h in flowing He, and then was cooled in flowing He at a rate of 180°C/h. After an equilibration, the surface and a polished cross-section of the sample were examined using a JEOL 5400 scanning electron microscope (SEM) to determine whether Pd_4S had formed. Energy dispersive spectroscopy (EDS) of microstructural features was done using a Voyager system from Thermo Electron Scientific Instruments Corp.

The microstructure of an ANL-3e sample showed clear evidence of reaction if Pd_4S formed during the equilibration. Figures 11 and 12 show samples that were equilibrated at 600 and 650°C in an atmosphere of 73% H_2/400 ppm H_2S/balance He to compare the microstructure when Pd_4S formed (Figs. 11a and 12a) to that when Pd_4S did not form (Figs. 11b and 12b). The sample equilibrated at 600°C (Fig. 11a) had a layer of Pd_4S (thickness ≈5 μm) on its surface and the familiar mixture of ceramic and metal phases beneath the reaction layer. In contrast, the typical mixture of ceramic and metal phases (Fig. 11b) extended all the way to the surface of the sample heated at 650°C, and there is no visible reaction layer. The difference in microstructure is also apparent in the plan views of the samples (Fig. 12). The sample heated at 600°C had a uniform appearance (Fig. 12a) because its surface had been covered by Pd_4S, but ceramic and metal phases were both visible in the sample heated at 650°C (Fig. 12b) because Pd_4S had not formed during the equilibration.

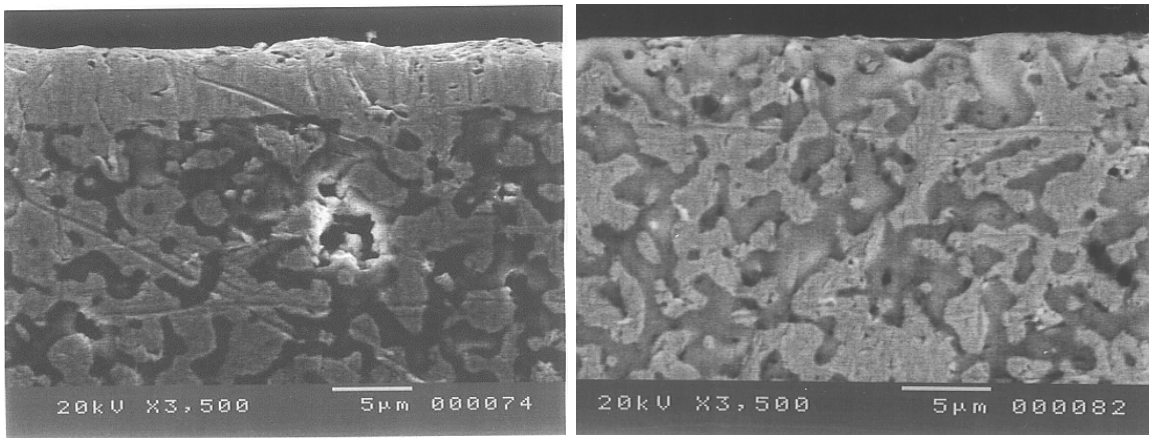

(a) (b)

Fig. 11 Cross-sectional backscattered electron images of ANL-3e membranes after exposure to 73% H_2/400 ppm H_2S/balance He for 50 h at: a) 600°C, and b) 650°C. Light-shaded areas are Pd or Pd_4S; dark-shaded areas are partially stabilized ZrO_2.

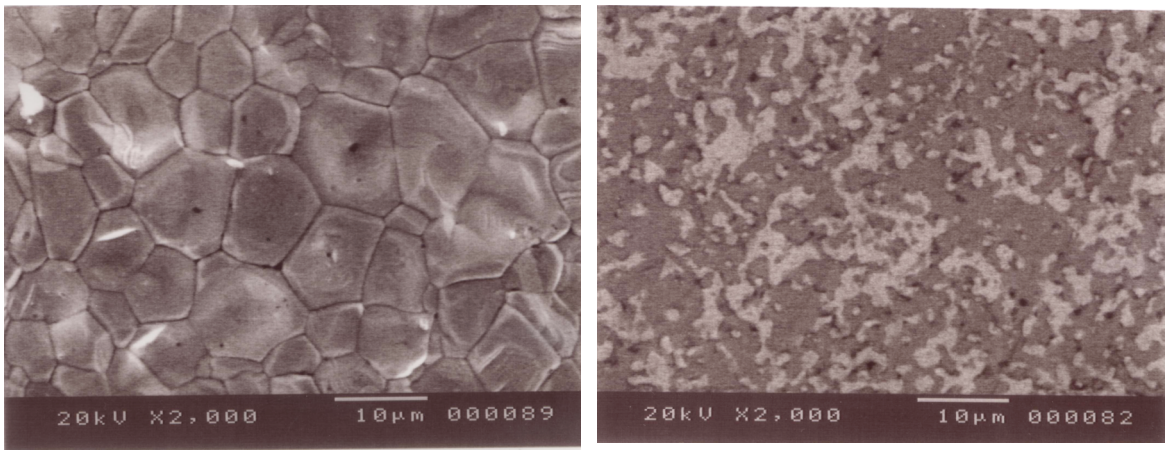

(a) (b)

Fig. 12 Backscattered electron images (plan views) of ANL-3e membranes after exposure to 73% H_2/400 ppm H_2S/balance He for 50 h at: a) 600°C, and b) 650°C. Light-shaded areas are Pd or Pd_4S; dark-shaded areas are partially stabilized ZrO_2.

We began studying the effect of syngas components using feed gas that contained 73% H_2/400 ppm H_2S/6.3% CH_4/6.8% CO_2/8.8% CO/balance He [7]. After equilibration at 700°C, an ANL-3e sample showed evidence that Pd_4S had formed, but there was no evidence of reaction after the equilibration at 650°C. These results contradicted Taylor's results [8] and our earlier results [1], which showed that Pd_4S is stable at temperatures below the Pd/Pd_4S phase boundary whereas Pd is stable at temperatures above the boundary. Because coke deposits were noted inside the furnace after the experiments at 650 and 700°C and it was unclear how coke formation altered the composition of the feed gas, use of this gas mixture was discontinued in subsequent experiments. Coke formation was avoided in later experiments by reducing the CH_4 content in the feed gas from 6.3% to ≤0.5%. Results that were obtained using a different feed gas with a lower CH_4 content did not contradict Taylor's results [8] or our earlier results [1], i.e., Pd_4S formed at temperatures below the Pd/Pd_4S phase boundary and not at temperatures above the boundary.

Figure 13 shows two types of information regarding the Pd/Pd_4S phase boundary: points that were calculated using thermodynamic data for the Pd-S system [8] and the $H_2/S_2/H_2S$ equilibrium [9], and data collected at Argonne by examining ANL-3e samples after they had been equilibrated in H_2/H_2S or "syngas"/H_2S mixtures. Bars with triangular symbols represent data collected at Argonne, with the symbols indicating whether the result was obtained using H_2/H_2S or "syngas"/H_2S mixtures, and the bars showing the temperature range in which the phase boundary is located. For a given H_2S concentration, the low-temperature end of a bar gives the highest temperature at which Pd_4S was found after an equilibration, whereas the high-temperature end of the bar gives the lowest temperature at which the membrane showed no sign of reaction, i.e., the lowest temperature at which Pd was stable. Each calculated point is a temperature at which Pd

and Pd_4S are in equilibrium for a given H_2 and H_2S concentration; Pd is stable at higher temperatures, whereas Pd_4S is stable at lower temperatures. To illustrate the effect of hydrogen concentration on the phase boundary (through the $H_2/S_2/H_2S$ equilibrium), points on the phase boundary were calculated for three H_2 concentrations. All data collected at Argonne to this point were collected using feed gases that contained 73% H_2.

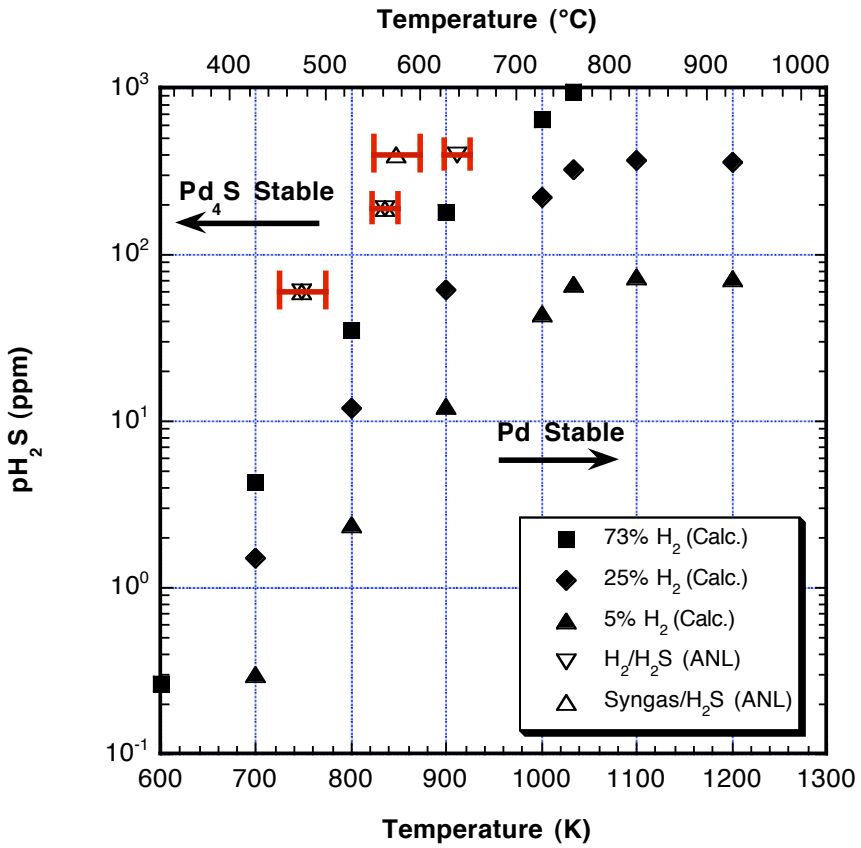

Fig. 13 Pd/Pd_4S phase boundary calculated for various H_2 concentrations using data from literature [8, 9]. Points with error bars summarize results obtained at Argonne by equilibrating ANL-3e samples at various temperatures in H_2/H_2S and "syngas"/H_2S mixtures.

Pd/Pd_4S phase boundary data collected at Argonne (Fig. 13) suggest that ANL-3e membranes should be stable in an atmosphere of 73% H_2/400 ppm H_2S/balance He at temperatures above ≈650°C. As the H_2S concentration decreases, membranes should remain stable down to lower temperatures, e.g., ≈500°C in gas that contains 60 ppm H_2S. At temperatures below the phase boundary, the formation of Pd_4S impedes hydrogen permeation through the membrane but does not necessarily destroy the membrane, as indicated by results given below showing that membranes can, in some cases, be regenerated after they have reacted with H_2S.

The phase boundary determined at Argonne is ≈50-75°C lower than the phase boundary calculated from thermodynamic data [8, 9]. This discrepancy between the

results is not large, especially considering that the thermodynamic data for the calculated phase boundary were extrapolated from higher temperatures (≈675-780°C). For H_2S concentrations of 60 and 190 ppm, the phase boundary in H_2/H_2S mixtures agreed with the phase boundary in syngas/H_2S mixtures, but the phase boundary for an H_2S concentration of 400 ppm was ≈50°C lower in the syngas/H_2S mixture than in the H_2/H_2S mixture. The reason for this difference for mixtures containing 400 ppm H_2S is not understood at this time.

Additional Results

A) Fabrication of HTM Thin Films

Because the hydrogen flux through ANL-3 HTMs is limited by bulk diffusion [3], reducing the membrane thickness should increase the hydrogen flux or allow the same flux at lower temperatures. To increase the hydrogen flux through HTMs and/or reduce their operating temperature, we are testing several methods for fabricating dense, thin-film membranes with thickness <10 μm. We previously used a paste-painting method to produce a 17-μm-thick ANL-3e membrane that gave the record high hydrogen flux for Argonne membranes [2]. Although the paste painting method is reproducible, a film thickness <10 μm is difficult to obtain with this method; therefore, we are developing the colloidal spray deposition (CSD) and spin-coating methods. In the CSD method, a colloidal suspension of membrane components is sprayed onto a porous substrate, whereas thin layers of membrane components are deposited in the spin-coating method by dripping a suspension onto a spinning porous substrate. Porous alumina substrates for thin-film membranes are prepared by pressing alumina hydrate powder into pellets that are pre-sintered at 800°C for 5 h in air. After the membrane layer is deposited by CSD or spin-coating, the substrate is heated to remove organic constituents from the membrane layer and densify the membrane film.

Thin films are tested for pinholes and/or microcracks by checking for penetration of the film by isopropyl alcohol (IPA). In the IPA-penetration test, several droplets of IPA are applied to the porous substrate (the "underside" of the film), and then the "topside" of the film is examined for evidence of penetration by the IPA. Penetration of the film by even small amounts of IPA is easily seen under an optical microscope as a darkening of the film.

i) Spin-coating

To prepare a thin film by spin coating, a colloidal suspension was made by mixing TZ-3Y powder from Tosoh and Pd powder (avg. particle size ≈1.0 μm) from Technic with an organic solvent, binder, plasticizer and dispersant. A relatively large amount (10 wt.%) of polyvinyl butyral binder improved the film's homogeneity and its adhesion to the substrate. Droplets of the suspension were applied to a substrate that was spun on a polishing wheel with a fixed spinning rate. Coated pellets were sintered for 5 h in ambient air at 1400-1450°C using heating and cooling ramp rates of 180°C/h.

Films prepared by spin coating showed good adhesion between the cermet film and the porous alumina substrate. No signs of delamination were seen during handling of the films or in SEM micrographs of the films. IPA-penetration tests showed penetration through a film sintered at 1400°C but no penetration through a film sintered at 1450°C. Figure 14 shows that the film sintered at 1450°C was uniform in thickness (≈25 μm) and had a randomly distributed metal phase. Further development of the spin coating method is focusing on we reducing the film thickness to ≤10 μm by controlling the viscosity of the suspension and the frequency of spin coating.

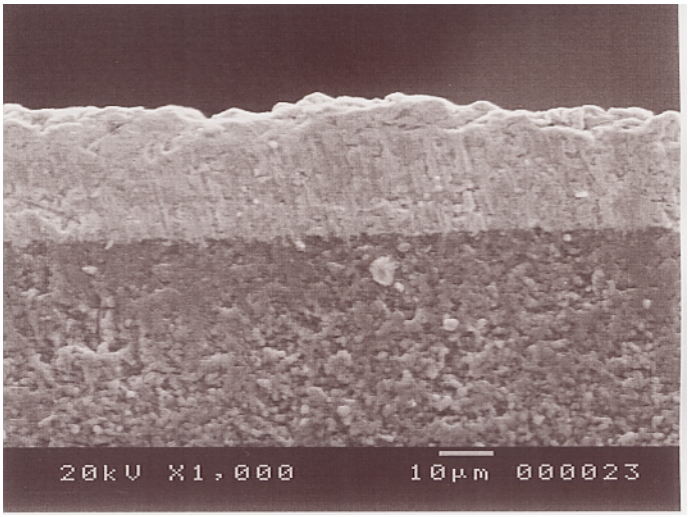

Fig. 14 Cross-sectional secondary electron image showing ANL-3e film made by spin coating method and sintered at 1450°C.

ii) Colloidal Spray Deposition (CSD)

To prepare ANL-3e thin films by CSD [10], a suspension was prepared using TZ-3Y powder and fine (avg. particle size ≈0.1 μm) Pd powder (Technic) coated with a binder to aid dispersion. The powders and an organic dispersant were mixed in water and ultrasonicated for 30 min to disperse the powders and break up agglomerates. To deposit a thin film, the ANL-3e colloidal suspension was delivered to an ultrasonic atomizing nozzle (Sono-Tek Corp.) by a programmable syringe pump and sprayed onto a partially sintered alumina substrate [2]. After the film was sprayed onto the substrate, it was dried on a hot plate. The green film and substrate were then sintered in ambient air at 1400ºC for 5 h using heating and cooling rates of 180ºC/h.

Figure 15 shows polished fracture surfaces of sintered films containing 50 (Fig. 15a) and 60 (Fig. 15b) vol.% Pd that were made by the CSD method. Both films appear dense and have a relatively uniform thickness (≈8-10 μm). Shortening the duration of colloidal spraying could decrease the film thickness further. After the films were sintered, they were tested for pinholes and/or micro-cracks using the IPA-penetration test described above. No penetration was observed in the film with 50 vol.% Pd, but IPA penetrated the film with 60 vol.% Pd, indicating the presence of connected porosity and/or cracks in the film.

SEM micrographs taken from the interior (Fig. 16a) and the surface (Fig. 16b) of the film with 60 vol.% Pd indicate that the Pd concentration is much lower at the surface than in the film interior. The low Pd concentration on the membrane's surface may be due to Pd evaporation during sintering at high temperature (1400°C) or to settling of Pd from the suspension during spraying. The loss of Pd must be minimized, because the membrane's hydrogen flux is directly related to its Pd content.

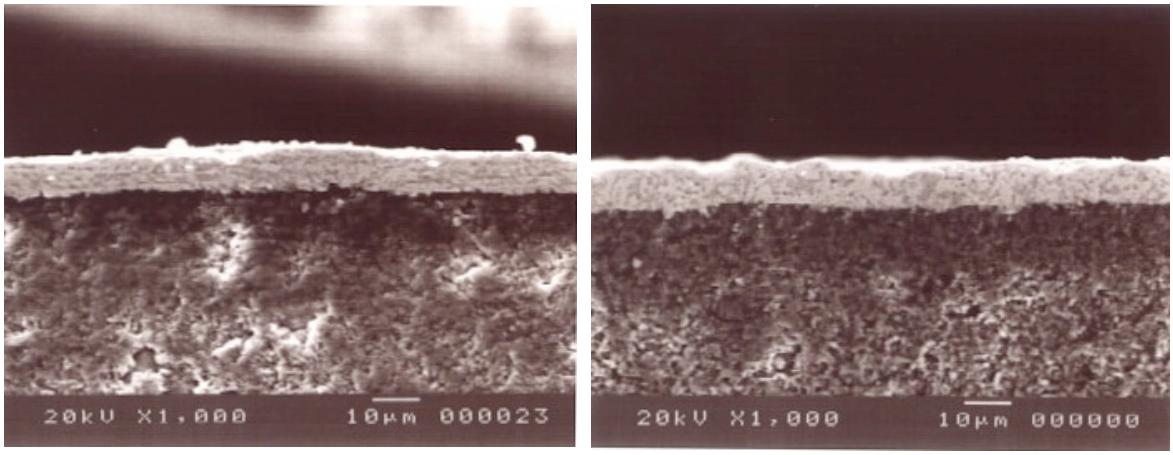

(a) (b)

Fig. 15 Cross-sectional secondary electron images of ANL-3e films made by colloidal spray deposition, containing a) 50 and b) 60 vol.% Pd.

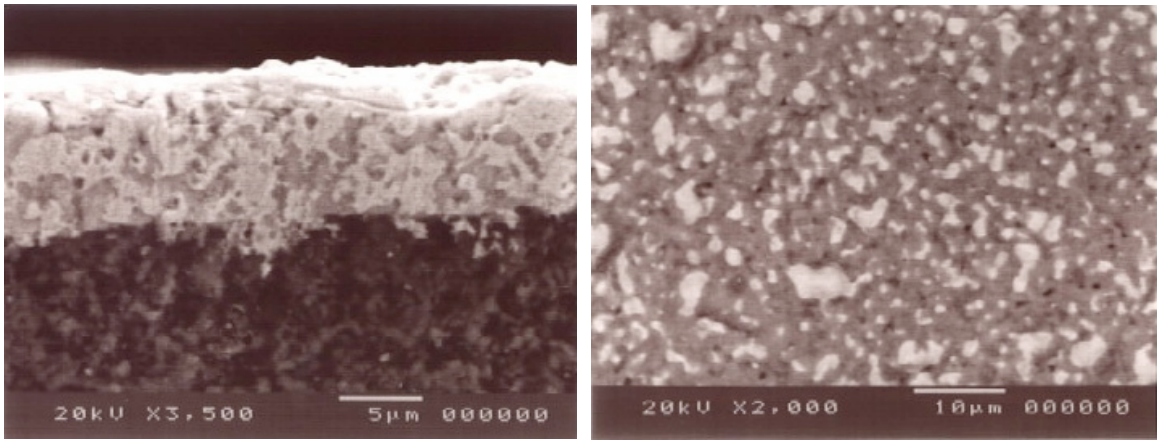

(a) (b)

Fig. 16 a) Cross-sectional and b) plan views of ANL-3e film with 60 vol.% Pd made by colloidal spray deposition method and sintered at 1400°C.

We used ultra-fine ceramic powder to prepare thin-film membranes by CSD in an attempt to reduce the loss of Pd by lowering the membrane's sintering temperature. The colloidal suspension was made using Pd powder (average particle size ≈0.1 μm) and nanometer-scale CeO_2 powder instead of TZ-3Y powder, which has an average particle size of ≈0.3-0.5 μm. A reduction in particle size increases the driving force for sintering and, in some cases, reduces the sintering temperature.

The suspension of CeO_2 and Pd powders was sprayed onto a partially sintered Al_2O_3 substrate and then sintered at 1400°C for 5 h using heating and cooling rates of 120°C/h. SEM micrographs after sintering show that the film appears fully dense (Fig. 17a) and had a thickness of ≈10-20 μm (Fig. 17b). CeO_2 appears in the surface-view (Fig. 17a) as smooth, rounded grains that underwent significant grain growth during sintering. The Pd grains seem composed of much smaller grains and have a rougher surface texture. The absence of pinholes in the Pd/CeO_2 film (Fig. 17a) contrasts with the microstructure of a Pd/TZ-3Y film (Fig. 16b). When Pd/CeO_2 and Pd/TZ-3Y films are both sintered at 1400°C, the Pd/CeO_2 film appears denser; however, when the sintering temperature is reduced even slightly (e.g., ≤1380°C), Pd/CeO_2 films also contain pinholes. In addition, chemical analysis of the film's surface using EDS showed that the Pd-content was still reduced during sintering of the Pd/CeO_2 thin film at 1380°C. This means that nanometer-scale CeO_2 powder probably does not provide the means to reduce Pd-loss during the sintering of ANL-3 membranes made by CSD.

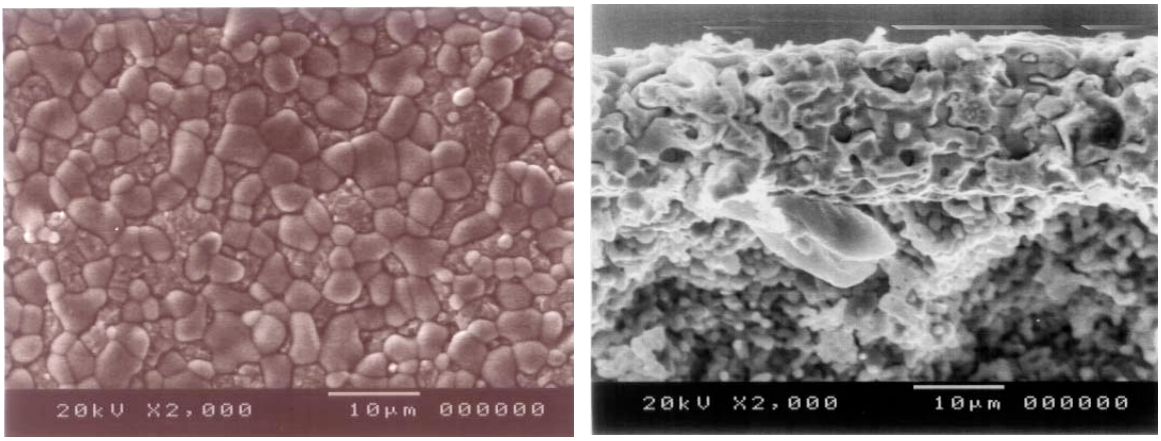

(a) (b)

Fig. 17 a) Plan, and b) cross-sectional views of Pd/CeO_2 thin film made on Al_2O_3 substrate by CSD and sintered at 1400°C/5 h.

Figure 18 compares the temperature dependence of hydrogen flux for a Pd/CeO_2 thin film fabricated by the CSD method and a Pd/TZ3Y thin film made by paste painting. The thickness of each film is shown in the plot. The Pd/CeO_2 film gives a lower flux due to the low Pd content on its surface. Because a material's vapor pressure increases as its particle size decreases, the low Pd content may be related to the fine Pd particle size in the Pd/CeO_2 film; therefore, we will explore the connection between Pd particle size and the microstructure and flux of ANL-3 thin films.

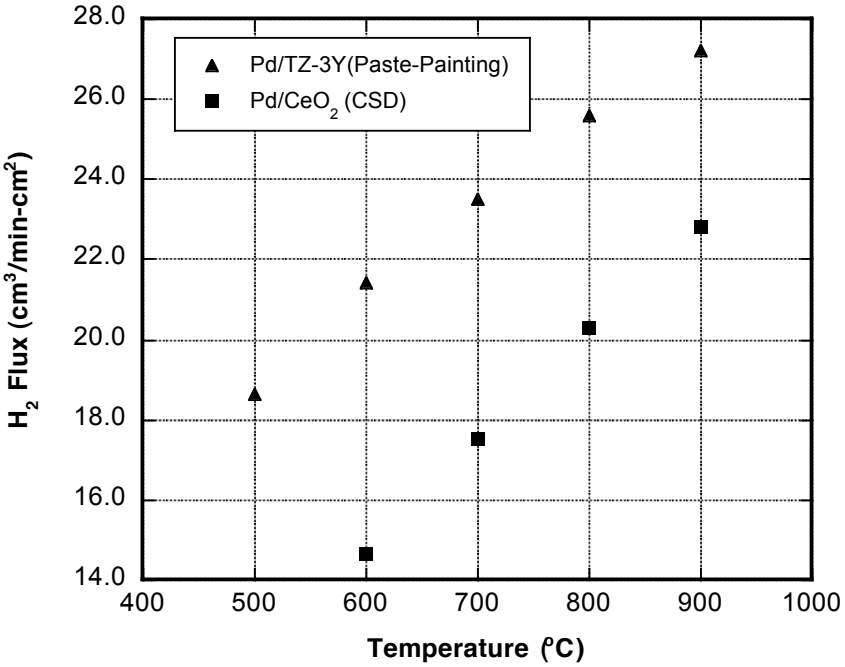

Fig. 18 H_2 flux for Pd/CeO_2 thin film made by CSD and Pd/TZ-3Y film made by paste-painting using 80%H_2/balance He as feed gas.

iii) Modified Thermal Method

In the thermal method for producing ANL-1a thin films [2], the composition of the atmosphere is precisely controlled during the sintering of BCY/NiO compacts so that kinetic limitations confine the reduction of NiO to the compact's surface. Because regions that contain Ni densify more easily than regions with NiO, only regions near the surface densify. NiO in the interior of the compact is not reduced during sintering, but porosity develops when NiO is subsequently reduced at a lower temperature. The modified thermal method combines aspects of the thermal method with the dip-coating method, in which a porous substrate is dipped into a colloidal suspension of thin film components that densify upon subsequent sintering. The modified thermal method was developed in order to improve control over film thickness and reduce the film's surface roughness.

To prepare BCY/Ni substrates, we pressed disks from a mixture of NiO, BCY, and graphite (5 wt. %) powders. The disks were heated at 800°C in air for 5 h to give them mechanical integrity for handling. Three preheated disks were coated one to three times with a colloidal suspension of BCY/NiO, and were dried at room temperature. The coated disks were heated to 1400°C in 200 ppm H_2/balance N_2 at a rate of 180°C/h, and were sintered at 1400°C in 4% H_2/balance N_2 for 0.1 h, then in 200 ppm H_2/balance N_2 for 9 h. After sintering, the BCY/NiO substrates were reduced by heating for 2 h at 800°C in 4% H_2/balance by N_2.

Figure 19 shows secondary electron images from fracture surfaces of samples after processing by the modified thermal method. In each case, a dense cermet film with uniform thickness formed on the porous BCY/Ni substrate. The film thickness increased

with the number of times that the substrate was coated with the BCY/NiO colloidal suspension. The film thickness was ≈14 μm after one coat (Fig. 19a), ≈26 μm after two coats (Fig. 19b), and ≈40 μm after three coats (Fig. 19c). The films were tested for connected porosity or microcracks using the IPA-penetration test, described above. The lack of penetration by IPA indicated that all three films were dense, and suggests that the thickness of dense cermet films can be reduced to ≈10 μm by controlling the coating and sintering processes.

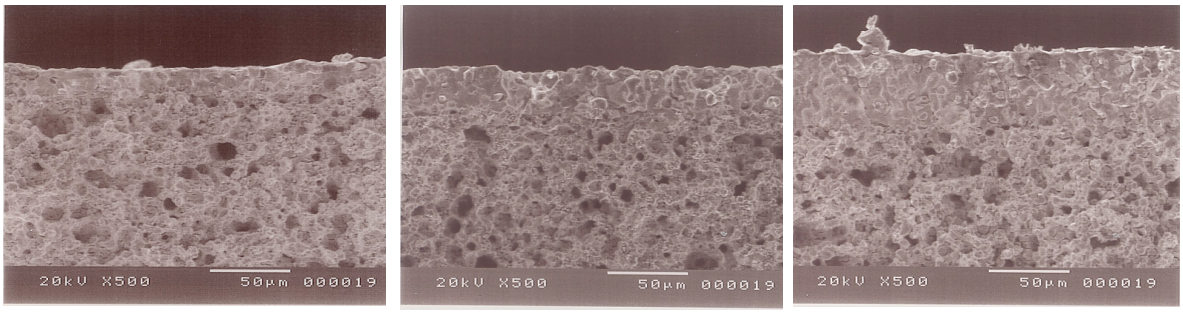

(a) (b) (c)

Fig. 19 Cross-sectional secondary electron images of ANL-1a films made by coating porous BCY/Ni substrates with BCY/NiO suspension (a) one time, (b) two times, and (c) three times.

B) High-Pressure Hydrogen Permeability Measurements at NETL

An ≈200-μm-thick ANL-3e membrane (50 vol.% Pd) was supplied to Mike Ciocco (NETL), who studied the effects of sweep gas flow rate and H_2 partial pressure in the feed gas (pH_2^{feed}) on the measured hydrogen permeability. The test conditions and results are listed in Table 3 in chronological order. The membrane was mounted in a modified VCR fitting, and then was positioned in NETL's HMT-2 test unit, as shown in Fig. 20.

Before mounting the membrane between two 1/16-in.-thick graphite gaskets, the sealing surfaces of the VCR fittings were machined flat. The membrane was heated at a rate of 120°C/hr with gas flow rates of 100 sccm He on the feed side and 100 sccm Ar on the sweep side. When the temperature reached 465°C, the feed gas was switched to 90% H_2/10% He. Feed gas mixtures of 3%, 5% and 90% H_2 were used in the tests, with a balance of helium in each case, and measurements were made at temperatures of 465, 635, and 765°C. Sweep gas flow rates were varied from 107 to 823 sccm.

After the membrane had been at operating temperatures for >200 h, the feed gas was switched to helium and the unit was cooled to ambient to accommodate a power shutdown. Upon reheating the unit to 465°C, the feed gas was switched to 5% H_2/He, at which point leaks were detected on both the sweep and feed side. Because the feed and sweep gases were leaking into the containment vessel and nitrogen was leaking into the feed and sweep streams, but feed gas was not leaking into the sweep stream, it was concluded that the leaks were through the graphite seals and not through the membrane itself. The leakage probably resulted from deformation of the sealing gaskets during temperature cycling; however, after the graphite seals were replaced and an attempt was made to resume testing, the membrane failed.

Table 3. Test conditions and results from permeation measurements made at NETL using ANL-3e membrane in chronological order.

Temp. (°C)	Condition Duration (h)	$\%H_2$ (%)	pH_2^{feed} (psia)	Feed Flow (sccm)	Sweep Flow (sccm)	Flux (mol/m^2-s)	Permeability (mol/m-s-Pa$^{1/2}$)
465	6.3	90	7.29	109	107	0.01355	8.14e-9
635	20.5	90	13.68	109	107	0.02326	1.24e-8
765	3.8	90	13.86	109	107	0.03020	1.64e-8
465	17.3	90	13.77	109	107	0.01417	7.32e-9
465	2.0	90	13.77	212	107	0.01429	7.40e-9
465	1.5	90	13.77	212	210	0.01463	7.34e-9
465	70.3	90	13.50	109	107	0.01218	6.28e-9
465	1.0	90	13.50	109	210	0.01439	7.26e-9
465	3.3	90	13.50	109	414	0.01504	7.44e-9
465	19.8	3	0.46	109	107	0.00176	5.58e-9
465	1.5	3	0.46	109	210	0.00191	5.70e-9
465	4.0	3	0.47	109	414	0.00225	6.46e-9
465	17.5	5	0.73	109	107	0.00221	5.34e-9
465	2.3	5	0.74	109	210	0.00250	5.72e-9
465	2.0	5	0.75	109	414	0.00271	5.96e-9
465	2.3	5	0.75	109	823	0.00266	5.70e-9
765	16.8	5	0.74	109	107	0.00440	1.16e-8
765	3.0	5	0.74	109	210	0.00497	1.22e-8
765	2.5	5	0.74	109	414	0.00548	1.27e-8
765	1.0	5	0.74	109	823	0.00602	1.35e-8
465	5.3	5	0.80	109	107	0.00243	5.80e-9
465	1.0	5	0.80	109	414	0.00284	6.18e-9

Figure 21 plots hydrogen permeability for this membrane and other Argonne membranes that were previously tested at NETL. The permeability of a Pd membrane is also shown as a baseline. Permeability values are compared, because each membrane had a different thickness (Pd: 1000 μm, ANL-648-66: 500 μm, ANL-655-137: 790 μm, and ANL-689-0156C: 200 μm). As shown in Fig. 21, the ANL-689-0156C results are very similar to the results for other Argonne membranes. The variations in results at 465°C (1/T = 0.00136 K^{-1}) and 795°C (1/T = 0.00096 K^{-1}) are due to changes in sweep flow rate and pH_2^{feed}.

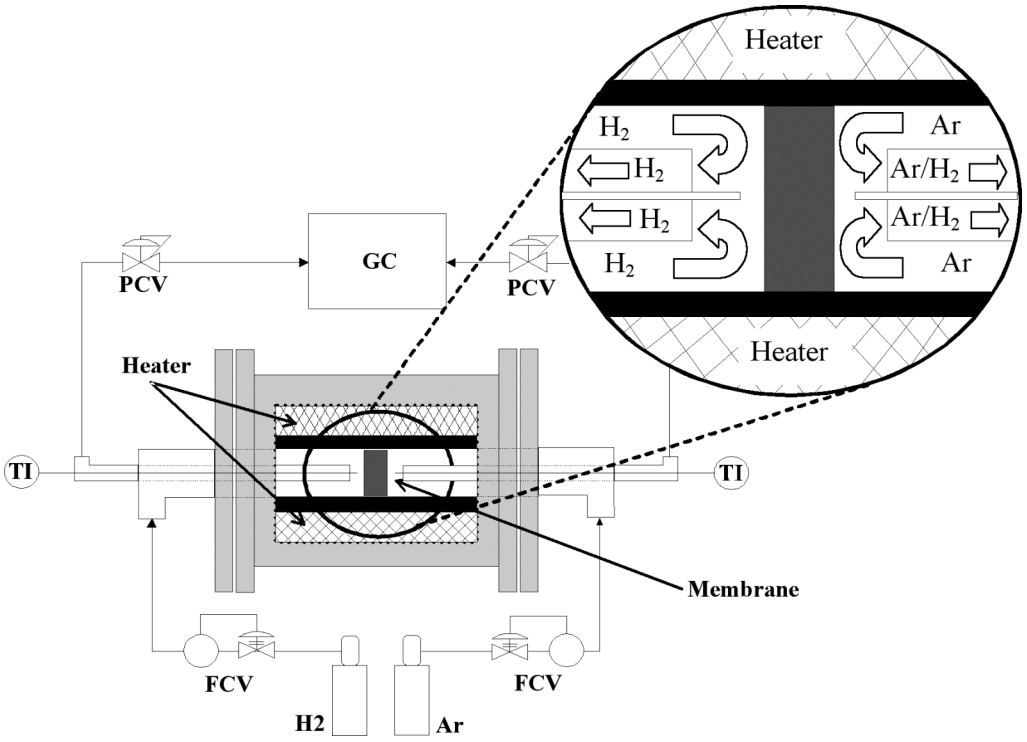

Fig. 20 Schematic of NETL's HMT-2 unit used to measure hydrogen permeability of ANL-3e membrane versus sweep gas flow rate and hydrogen partial pressure in feed gas.

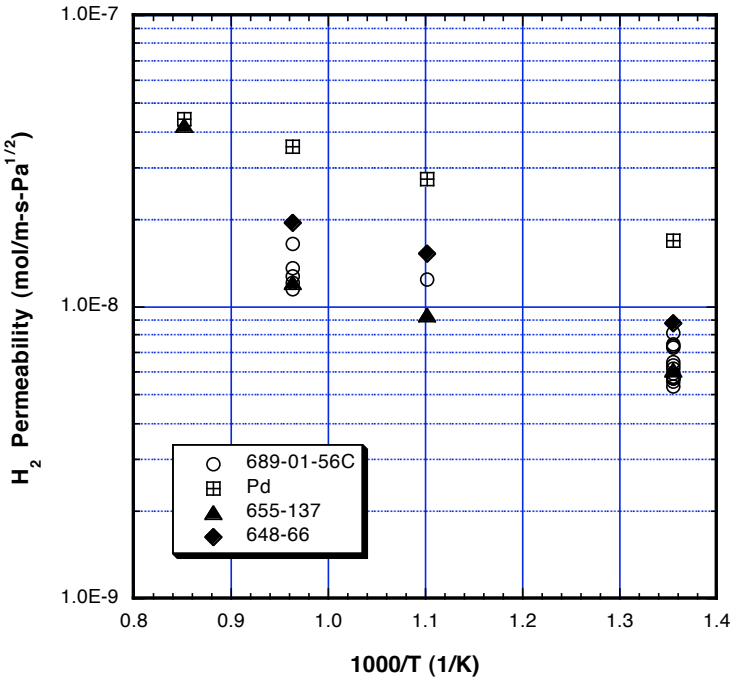

Fig. 21 H_2 permeability of ANL-3 membranes (655-137, 648-66, and 689-01-56C, the most recent sample) and Pd membrane, measured at NETL.

The effects of sweep flow rate and pH_2^{feed} are shown in Fig. 22. The permeability values measured with feed gas of 90% H_2 were slightly higher than values obtained using either 3% or 5% H_2 as the feed gas. A plausible explanation for this difference is concentration polarization on the feed side of the membrane. With low pH_2^{feed}, the feed gas can be depleted of H_2 in a boundary layer next to the membrane, which decreases the effective pH_2 at the feed surface. Increasing the feed gas flow rate can mitigate this effect; therefore, the effect of feed gas flow rate will be studied in a future test. Note that the feed gas flow rate differed by a factor of two in two measurements made at 465°C with 90% H_2 as the feed gas. In this case, the difference in flow rate had no effect on the permeability, as shown in Table 3. This might not be surprising, however, because the high concentration of H_2 (90%) in these tests would make the depletion of H_2 in the feed stream nearly impossible.

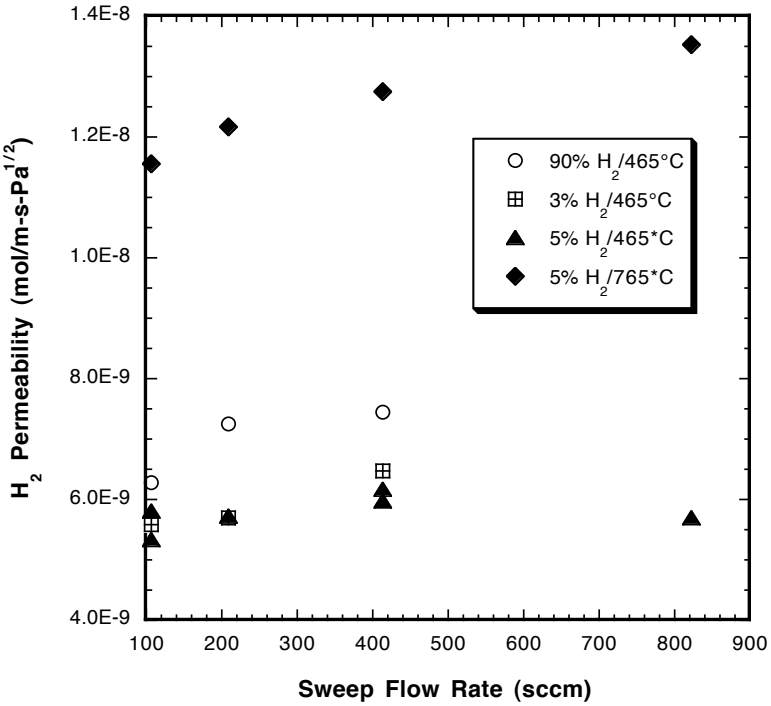

Fig. 22 H_2 permeability of ANL-3e membrane (689-01-56C) vs. sweep flow rate using various feed gases at 465 and 765°C, all gases balanced by He. Measurements were made at NETL.

As shown in Fig. 22, the sweep flow rate had very little, if any, effect on the permeability at 465°C when the feed gas contained lower H_2 concentrations (3% and 5%). However, the permeability appeared to increase slightly when the sweep flow rate was increased at 765°C with either 5% H_2 or 90% H_2 as the feed gas. This might indicate concentration polarization from accumulation of H_2 near the sweep surface of the membrane, which gives a higher pH_2 near the sweep surface of the membrane than in the sweep stream away from the membrane. As a result, the actual driving force for hydrogen permeation is smaller than the calculated driving force $(\sqrt{pH_2^{feed}} - \sqrt{pH_2^{sweep}})$, and the measured permeability value is lower than the calculated value. Increasing the sweep flow rate can alleviate concentration polarization by preventing the accumulation of H_2.

C) Regeneration of ANL-3e Membrane after Attack by H_2S

To test whether a membrane's performance can be "regenerated" after the membrane has reacted with H_2S, we measured a sample's flux while the feed gas was switched from 73% H_2/400 ppm H_2S/balance He to 73% H_2/balance He (no H_2S). The experiment was conducted at 600°C, because Pd_4S forms at this temperature in gas containing 73% H_2/400 ppm H_2S/balance He [1]. Following procedures that are described elsewhere [3], flat gold rings were used as seals, and the hydrogen flux was measured using either 73% H_2/400 ppm H_2S/balance He or 73% H_2/balance He (no H_2S) as the feed gas. For a given condition, the hydrogen and helium concentrations in the sweep stream were measured 2-4 times using a gas chromatograph (SRI 8610C), and the average of those readings was used to calculate the hydrogen flux. Individual readings varied from the average value by ≤10%. The values of hydrogen flux were corrected for leakage based on the measured helium leakage rate.

Table 4 summarizes the sequence of atmospheres to which the sample was exposed during the experiment. Beginning with 73% H_2/balance He (no H_2S) as the feed gas, the initial flux (time=0 h) was measured, after which the feed gas was switched to 73% H_2/400 ppm H_2S/balance He and the flux was monitored for ≈114 h. After ≈114 h, the feed was switched back to 73% H_2/balance He (no H_2S), and the flux was monitored for ≈172 h. In this way, the flux was measured for a total of ≈1000 h while the feed was alternated between H_2S-containing and H_2S-free gases. During the experiment, the sample was exposed to H_2S-containing gas four times and was regenerated three times in H_2S-free gas.

Table 4. Sequence of feed gas compositions used to test whether an ANL-3e membrane can be "regenerated" after its corrosion by H_2S.

Atmosphere	Start Time (h)	End Time (h)
73% H_2/**400 ppm H_2S**/balance He	0.0	113.8
73% H_2/balance He (**no H_2S**)	113.8	286.2
73% H_2/**400 ppm H_2S**/balance He	286.2	376.9
73% H_2/balance He (**no H_2S**)	376.9	474.2
73% H_2/**400 ppm H_2S**/balance He	474.2	621.9
73% H_2/balance He (**no H_2S**)	621.9	835.5
73% H_2/**400 ppm H_2S**/balance He	835.5	1028.3

Gas mixtures were prepared using mass flow controllers (MKS 1179A) to blend appropriate amounts of three gases: He, H_2, and 1240 ppm H_2S/balance H_2. The flow rate of the gas mixtures was 200 cm^3/min, and the chamber holding the sample during the equilibration had a volume of ≈2600 cm^3. Therefore, a volume of gas equivalent to the chamber volume flowed into the chamber in ≈13 min, and the gas composition in the sample chamber reached the feed gas composition within ≈1 h after changing the feed gas composition.

Figure 23 shows the time dependence of hydrogen flux and leakage, as indicated by the He concentration measured in the sweep gas. The flux quickly decreased during each exposure to H_2S-containing feed gas, presumably due to the formation of Pd_4S on its surface. Each time the feed was switched to H_2S-free gas, however, the flux recovered equally quickly. Interestingly, the flux actually increased after the first H_2S-exposure and regeneration from an initial value of 0.96 $cm^3/min\text{-}cm^2$ (t=0 h) to 1.30 $cm^3/min\text{-}cm^2$ at t≈195 h. The leakage increased during the experiment, but only slightly and not nearly enough to account for the increase in hydrogen flux. These results indicate that ANL-3e membranes can, in some cases, be regenerated after they have been degraded by H_2S.

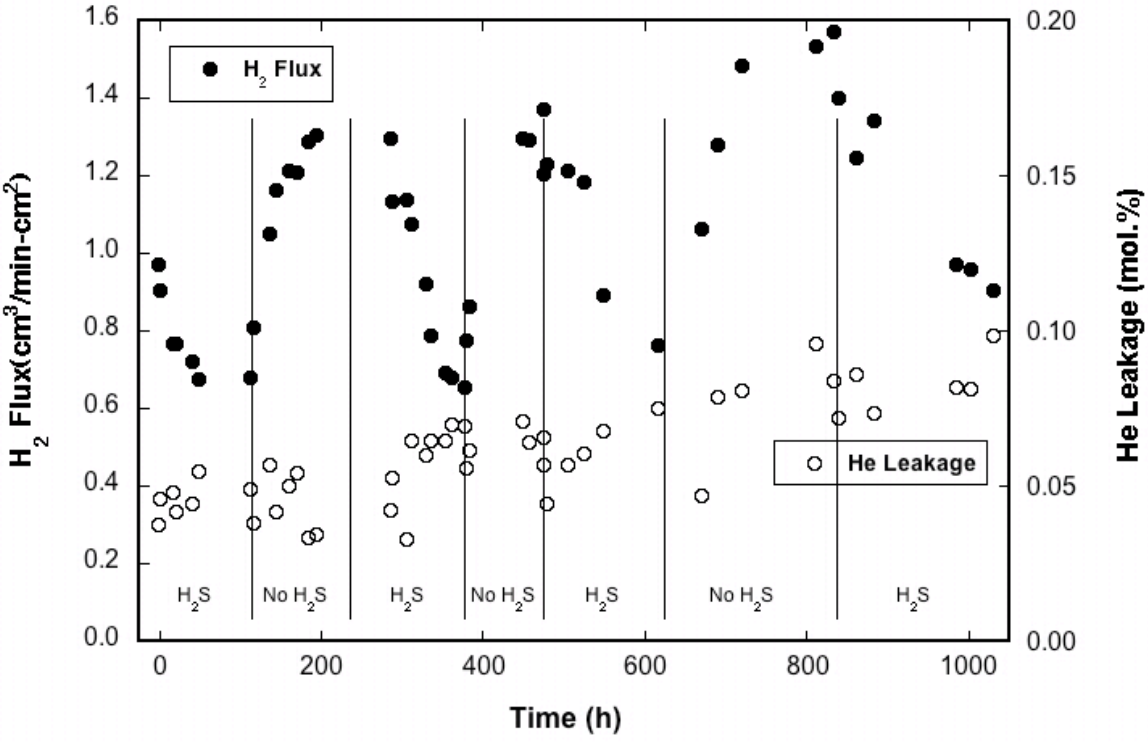

Fig. 23 H_2 flux and He leakage at 600°C for ANL-3e membrane as feed gas was alternated between 73% H_2/400 ppm H_2S/balance He, indicated in graph by "H_2S", and 73% H_2/balance He, indicated by "No H_2S." Details of feed gas composition are given in Table 4.

After the experiment, a cross-section of the sample (Fig. 24a) showed a layer of Pd (thickness≈20 μm) on the membrane's feed surface and more porosity near the feed side than near the sweep side. A plan view (Fig. 24b) showed that the layer of Pd was dense except for isolated porosity. The post-test images clearly indicate that Pd diffused from the membrane's interior to the feed surface during the membrane's reaction with H_2S. Assuming that the surface layer of Pd is dense, as it seems in Fig. 24, the migration of Pd to the surface decreases the effective thickness of Pd, because TZ-3Y is not mixed with Pd on the surface but is mixed with Pd in the membrane's interior. Such a decrease in the effective thickness of Pd might explain the increase in hydrogen flux that resulted from the H_2S-exposure and subsequent regeneration of the membrane.

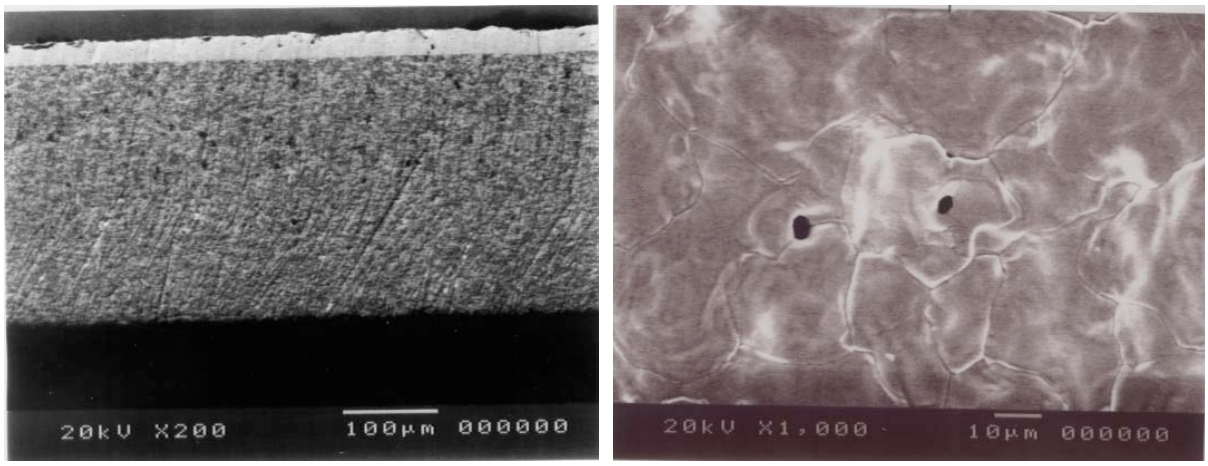

(a) (b)

Fig. 24 a) Cross-sectional, and b) plan views of ANL-3e membrane after testing whether it could be "regenerated" after corrosion by H_2S. Details of feed gas compositions are given in Table 4.

D) Hydrogen Production via Water Splitting With OTM

Water dissociates at high temperatures, but very low concentrations of hydrogen and oxygen are generated even at relatively high temperatures (>1600°C), because the equilibrium constant for dissociation is small. However, significant amounts of hydrogen can be generated at moderate temperatures (500-900°C) if an OTM is used to remove oxygen as it is generated. We demonstrated this previously [11] using self-supported ANL-1b membranes composed of Gd-doped CeO_2 (CGO) and Ni. If the surfaces of the OTM are prepared appropriately, limitations from surface reaction kinetics can be greatly minimized, in which case enhancing oxygen transport through the OTM can increase the hydrogen production rate. To enhance oxygen transport through OTMs, the thickness of the OTM can be reduced, and/or an OTM with intrinsically faster oxygen permeation rates can be used. During FY 2006, we studied the effect of thickness on hydrogen production using OTMs composed of $Sr_{1.0}Fe_{1.0}Co_{0.5}O_x$ (SFC2), whose oxygen transport is faster than that of CGO/Ni, and we used the modified thermal method to reduce the OTM thickness by fabricating thin films on porous substrates.

i) Hydrogen Production Using SFC2 as OTM

The ANL-0b OTM is composed of SFC2 and yields a hydrogen production rate at 900°C that is ≈2 times higher than that of the ANL-1b OTM [12]. Our previous study of the ANL-0b membrane showed that its hydrogen production rate at 900°C might be limited by the surface oxygen exchange kinetics [13]. To clarify whether the hydrogen production rate of ANL-0b is limited by bulk or surface kinetics, we measured the hydrogen production rate as a function of membrane thickness (0.21-0.98 mm). Hydrogen production rate measurements were made at 900°C with pH_2O=0.49 atm on the hydrogen-generation side of the membrane and pH_2=0.8 atm on the oxygen permeate side.

The hydrogen production rate of ANL-0b varies linearly with the inverse of membrane thickness (Fig. 25), increasing from 5.0 $cm^3/min\text{-}cm^2$ with a 0.98-mm-thick membrane to 7.6 $cm^3/min\text{-}cm^2$ using a 0.21-mm-thick membrane. The linear relationship is consistent with the hydrogen production rate being limited by oxygen permeation through the bulk of the membrane. Extrapolation of the hydrogen production rate does not pass through the origin, however, which indicates that surface reaction kinetics also influence the data. The hydrogen production rate for the 0.21-mm-thick membrane was only 50% larger than that for the 0.98-mm-thick membrane. If hydrogen production were limited only by oxygen permeation through the membrane's bulk, the production rate for the thinner membrane should be ≈five times larger than that of the thicker membrane.

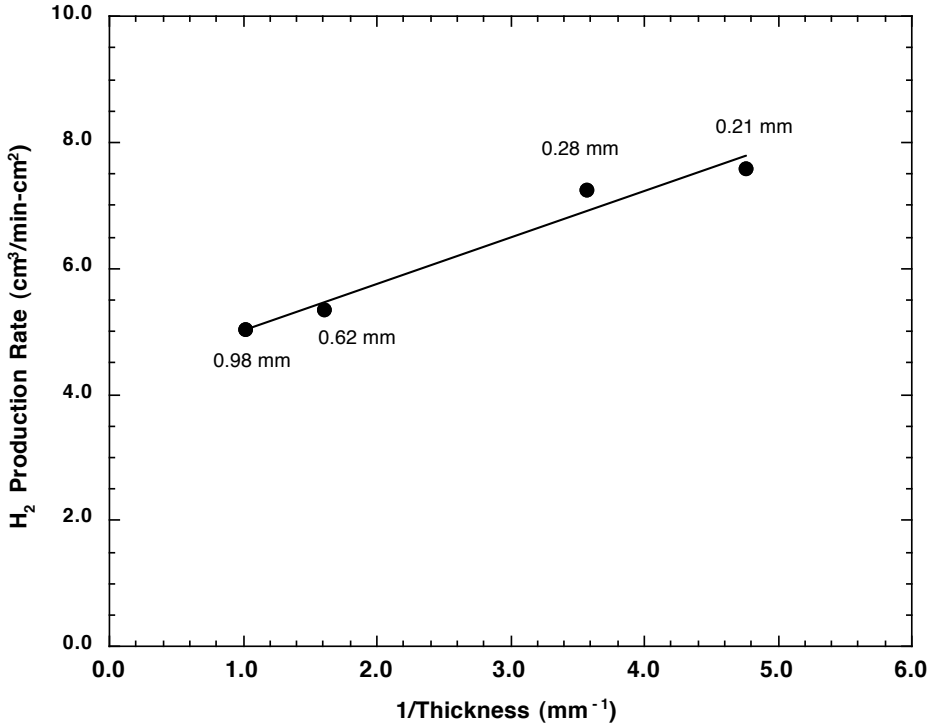

Fig. 25. H_2 production rate vs. inverse of membrane thickness for ANL-0b membranes at 900°C using wet pH_2O = 0.49 atm on hydrogen-generation side of membrane and pH_2 = 0.8 atm on oxygen permeate side. Membrane thickness is given in the figure.

Limitations from surface reaction kinetics are also evident in the variation of hydrogen production rate with pH_2 on the oxygen-permeate side of the membrane, shown in Fig. 26. The measurements were made at 900°C with pH_2O=0.49 atm on the hydrogen-generation side of the membrane. The hydrogen production rate increased with increasing pH_2 on the oxygen-permeate side, as expected, but it deviated from a logarithmic dependence on pH_2. By contrast, a logarithmic dependence was obtained in our study with ANL-1b membranes [13] when we minimized the limitations from surface reaction kinetics by adding porous layers to the membrane. The deviation from a logarithmic dependence (Fig. 26) suggests that the hydrogen production rate is partially limited by the kinetics of oxygen exchange on the surface of the ANL-0b membrane.

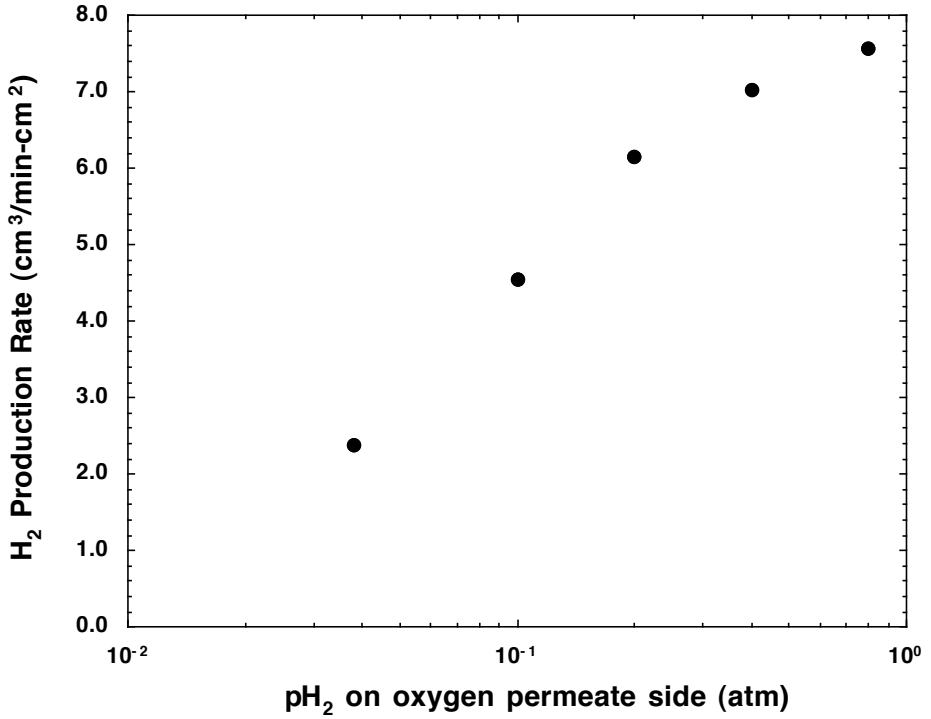

Fig. 26. H_2 production rate of 0.21-mm-thick ANL-0b membrane at 900°C using wet N_2 (pH_2O = 0.49 atm) on H_2-generation side.

ii) Fabrication of OTM Thin Films

The data in the previous section and previous work [14] show that higher hydrogen production rates by OTMs might be achieved by decreasing the membrane thickness. In order to produce thinner (<50 μm) membranes with sufficient mechanical integrity for routine handling, we are testing several methods for fabricating dense thin films on porous substrates. In the dip-coating method, a porous substrate is dipped into a colloidal dispersion of thin film components that densify during sintering, whereas the thermal method induces a dense thin film to form by controlling the gas phase during sintering. The modified thermal method combines aspects of the dip-coating and thermal methods, and was developed in order to improve control over film thickness and reduce the film's surface roughness. The modified thermal method was tested during FY 2006 for fabricating several OTM thin film/substrate combinations (CGO/Ni thin film on porous BCY/Ni and SCF2/Ni thin film on porous CGO/Ni).

BCY/Ni was chosen as a porous support for CGO/Ni thin films, because it was used to successfully fabricate BCY/Ni thin films, and BCY/Ni is believed to catalyze the dissociation of water. BCY/NiO substrates were prepared using the procedure given above in the section that describes the modified thermal method. After being pre-sintered at 800°C in air, BCY/NiO disks were coated with CGO/NiO colloidal suspension and dried at room temperature. Coated disks were heated to 1400°C at a rate of 180°C/h in 200 ppm H_2/balance N_2, and were sintered at 1400°C in 4% H_2/balance N_2 for 0.3 h followed by 9 h in 200 ppm H_2/balance N_2. To fully reduce NiO in the substrate after sintering, the coated disk was heated at 800°C in 4% H_2/balance by N_2 for 2 h. The substrate composition was controlled to give 40 vol.% Ni after reduction. Figure 27

shows secondary electron images from a fracture surface of a sintered CGO/Ni film on a porous BCY/Ni substrate. The CGO/Ni cermet film has uniform thickness (≈40 μm) and appears dense, which was confirmed by the IPA-penetration test.

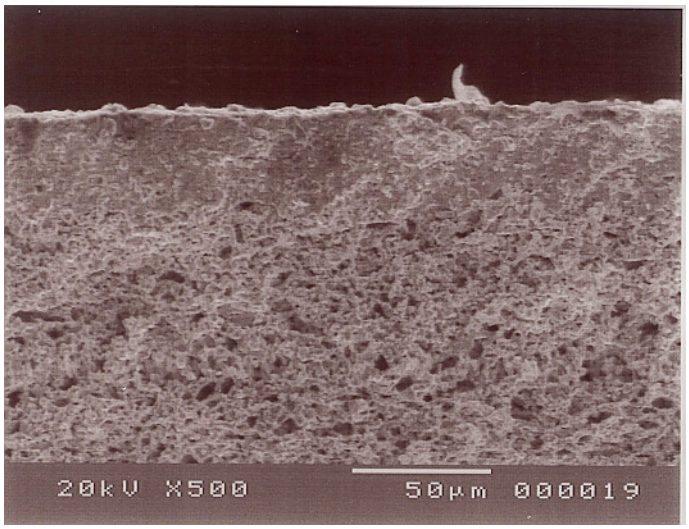

Fig. 27 Secondary electron image from fracture surface of CGO/Ni film made by the modified thermal method on porous BCY/Ni substrate.

We are developing methods to fabricate SFC2 thin films on porous substrates, because SFC2 is a good oxygen separation membrane that yields high hydrogen production rates [2]. Initially, SFC2 films were prepared on porous SFC2/Ni substrates made by a process like that described above for BCY/Ni substrates. SFC2 and NiO powders were mixed with graphite (7 wt.%) as a pore former, pressed into disks, and then pre-sintered at 800°C in air for 5 h. An SFC2 colloidal suspension was cast onto the pre-sintered SFC2/NiO disk, and then the coated disk was sintered at 1200°C for 10 h in air. Plan and cross-sectional views of an SFC2 film are shown in Fig. 28 before the substrate was reduced by heating the sample at 900°C in 4% H_2/balance by N_2. Several isolated, elongated pores in the substrate indicate that the pore-forming graphite powder was not homogeneously distributed. The SFC2 film appears dense and crack-free; however, the sample curled badly when it was reduced, and it could not be tested.

Unlike SFC2/Ni substrates, CGO/Ni substrates did not deform during reduction, therefore, SFC2 was deposited onto a CGO/NiO disk that was prepared by the procedure described above. The coated disk was heated up to 1300°C in 200 ppm H_2/balance N_2 at a rate of 180°C/h, and was sintered at 1300°C in 4% H_2/balance N_2 for 0.1 h, and then in 200 ppm H_2/balance N_2 for 9 h. The CGO/NiO substrate was then reduced by heating the sample at 900°C in 4% H_2/balance by N_2 for 2 h. Using this process, a dense SFC2 film (≈15 μm thick) was formed on porous CGO/Ni. The sample did not curl during fabrication, and the IPA-penetration test showed no evidence of cracks or interconnected porosity. Another SFC2 film on porous CGO/Ni was made in order to measure its hydrogen production rate; however, a good gas seal was not obtained. When the sample was removed from the furnace, the SFC2 film had peeled away from the substrate.

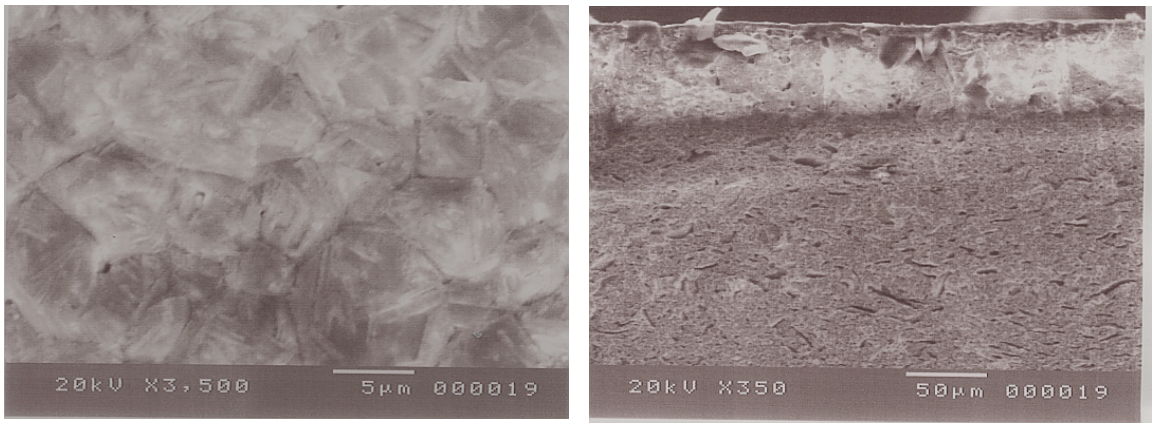

(a) (b)

Fig. 28. a) Plan, and b) cross-sectional views of sintered SFC2 film made by modified thermal method on porous SFC2/Ni substrate.

To improve adhesion between the film and substrate, NiO was added to the composition of the thin film, and SFC2/NiO was deposited onto the CGO/NiO substrate. The sintering and reduction conditions remained the same as those used to fabricate SFC2 films. A polished cross section of a sample (Fig. 29) shows a dense SFC2/Ni film on a porous CGO/Ni substrate. In a sign of improved adhesion between the film and substrate, a SFC2/Ni film did not peel from its CGO/Ni substrate during exposure to the ambient atmosphere for more than one month, whereas an SFC2 film peeled from its on CGO/Ni substrate after several days.

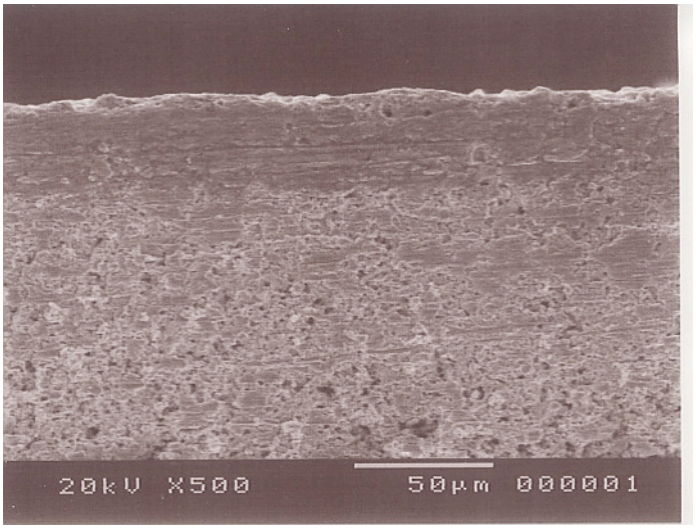

Fig. 29 Secondary electron image from polished fracture surface of SFC2/Ni film made by modified thermal method on porous CGO/Ni substrate.

E) Effect of Steam on Hydrogen Flux of ANL-3e Membrane

In evaluating the chemical stability of HTMs, we studied the effect of water vapor on the hydrogen flux of an ANL-3e membrane (Pd/TZ3Y, 50 vol.% Pd) with a thickness of 0.22 mm. The disk-shaped membrane was sintered at 1480°C for 10 h in air, and then both faces were polished with 600-grit SiC paper. The hydrogen flux was measured at 600 and 900°C using sweep gas of ultra high purity (UHP) N_2 flowing at a constant rate of 150 cm^3/min. The feed gas (50% H_2/balance UHP He) flowed in a "dry" condition, i.e., directly from the gas cylinder, or was bubbled through a water bath (EX-35D1 from Fisher Scientific) at a temperature of 25-81°C to give feed gas with a partial pressure of water (pH_2O) of 0.03-0.49 atm.

Figure 30 shows hydrogen flux versus the partial pressure of water (pH_2O) in the feed gas. Each point for moist feed (i.e., 0.03, 0.07, 0.18, and 0.49 atm H_2O) represents the average of three or four separate measurements made over a period of 0.5-1.0 h, during which time the hydrogen flux showed no significant change. Although 0.5-1.0 h is a relatively brief period, it is expected that an ongoing reaction of the membrane would cause a discernible change in the flux. Before each measurement in a moist condition, the flux was measured in dry feed gas to confirm that the previous exposures to moisture had not caused irreversible changes to the membrane. The points for dry feed gas (at 600 and 900°C) give the average of all the flux values that were measured before and after each exposure to moisture at the respective temperatures. The good reproducibility of "dry" flux values indicates that moisture did not irreversibly change the membrane, and the steadiness of flux values during "moist" measurements suggests that the ANL-3e membrane is stable during exposure to moisture (up to 0.49 atm H_2O).

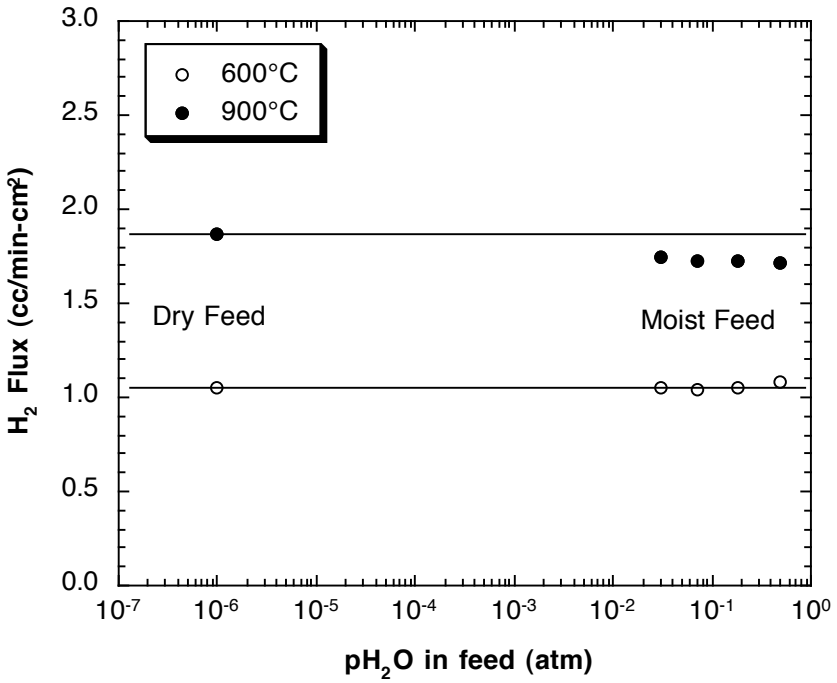

Fig. 30. Water vapor pressure dependence of hydrogen flux at 600 and 900°C for ANL-3e membrane (≈0.22 mm thick).

The hydrogen flux was independent of pH_2O in the feed gas at 600°C, but showed a slight systematic decrease versus pH_2O in the feed gas at 900°C. The decrease at 900°C is probably not caused by water vapor occupying absorption sites on the Pd surface and creating a barrier to H_2 absorption, because a similar decrease would be expected at 600°C if this were the case. Oxygen diffusion through TZ-3Y, a known oxygen ion conductor, might explain the decrease in hydrogen flux at 900°C, however. Oxygen that is produced by water dissociation in the feed gas could permeate to the sweep side of the membrane, where it would react with permeated hydrogen. In addition, the diffusion of oxygen ions through TZ-3Y would be coupled with the diffusion of electrons through Pd, which might impede the permeation of hydrogen. Due to the thermally activated nature of oxygen permeation, these effects would be expected to influence the hydrogen flux more at 900°C than at 600°C.

V. FUTURE WORK

The Aspen Plus® Simulation module will be used to evaluate the economics of an IGCC hydrogen production system that utilizes HTMs for hydrogen purification. In our evaluation, we will compare the economics of an IGCC system operating at 900°C to one operating at 400°C. In addition to identifying novel equipment, estimating its cost, and considering challenges with interfacing the equipment with the overall system, we will explore opportunities to optimize the overall process. In particular, heat source temperature, pressure and duty requirements, heat carrier medium, and conditions and purity of the process streams will be considered in the evaluation. While most of the plant will be based on well-understood equipment, we will need to develop user modules for the HTM units, because they represent a departure from commonly used equipment.

We will begin fabricating tubular HTMs in order to increase their effective area and demonstrate that they can be made into practical devices. Several methods will be explored for fabricating HTM tubes. They will be fabricated as monolithic tubes, i.e., the entire tube will be composed of HTM components or as HTM thin films that are deposited on porous tubular supports. Various methods (dip-coating, spray deposition, paste-painting) will be tested to identify an effective way to deposit dense HTM thin films on porous tubes. To evaluate the performance of the HTM tubes, we will develop methods for manifolding the tubes while obtaining a gas-tight seal. In other tests, e.g., evaluating chemical stability and measuring hydrogen flux at high pressure, we will continue to use small disk-shaped samples.

Because H_2S is an important contaminant that degrades Pd-containing HTMs by forming Pd_4S, we will continue determining the position of the Pd/Pd_4S phase boundary to identify conditions under which Pd_4S forms. To this point, we have determined the phase boundary using feed gases in which the H_2 concentration has been held constant ($\approx$73% H_2). We will begin locating the phase boundary using feed gases with a lower H_2 concentration, because the H_2 concentration affects the position of the phase boundary.

In order to understand the effect of feed gas composition (the H_2 and H_2S concentrations) on the performance of HTMs, we will correlate hydrogen flux measurements with the phase boundary data. In particular, we will compare hydrogen flux measurements that are made when Pd_4S is stable to flux measurements that are made when Pd is stable.

We will continue using Argonne's high-pressure reactor to study the performance of Argonne membranes and seals at high pressures. We replaced the hydrogen sensor that limited our initial high-pressure measurements to $\Delta pH_2^{1/2}$ values of $\approx$0.7 $atm^{1/2}$; therefore, it will be possible to measure hydrogen flux using $\Delta pH_2^{1/2}$ values approaching $\approx$3.5 $atm^{1/2}$. Because NETL's high-pressure measurements (described above) suggest that the flow rates of feed and sweep gases might influence the flux under some conditions, we will investigate the effects of sweep and feed gas flow rates during our high-pressure flux measurements.

We will continue efforts to improve the properties of Argonne's HTMs. Because the hydrogen flux and chemical stability of ANL-3 membranes depend primarily on the properties of the hydrogen transport metal, we will continue testing metals to increase hydrogen flux, improve chemical stability, and/or reduce membrane cost. We will test binary alloys, and possibly ternary alloys, depending on the results obtained with the binary alloys. The hydrogen flux through newly developed membranes will be measured as a function of temperature for short-term (several hours) exposures to hydrogen-containing gases. The chemical stability of membranes will be assessed by monitoring their hydrogen flux during brief (24-48 h) exposure at 400-600°C to gases that are typical for IGCC processes. We will work to improve the methods for fabricating thinner, stronger, defect-free thin films. Membrane surfaces will be characterized using NETL's in-house facilities.

Evaluation of process issues and economics will continue as technical progress warrants. As directed though consultations with NETL's program managers, contacts will be made and discussions will be held with potential collaborators. We will work with NETL's in-house R&D team and their Systems Engineering group to validate the process concept and conduct techno-economic evaluation of proton-conducting membrane technology for separating hydrogen in the power and petrochemical industries. We will provide technical input and engineering data to the NETL team to develop models for process viability and for thermal management studies.

VI. PUBLICATIONS, PRESENTATIONS AND PATENTS

Transport Properties of $BaCe_{0.95}Y_{0.05}O_{3-a}$ Mixed Conductors for Hydrogen Separation, Solid State Ionics, 100, 45 (1997).

Development of Mixed-Conducting Oxides for Gas Separation, Solid State Ionics, 108, 363 (1998).

Development of Proton-Conducting Membranes, presented at the AIChE Annual Meeting, New Orleans, LA, March 9-13, 1998.

Mixed-Conducting Ceramic Membranes for Hydrogen Separation, presented at the 193rd Meeting of the Electrochemical Society, San Diego, CA, May 3-8, 1998.

Development of Mixed-Conducting Ceramic Membranes for Hydrogen Separation, Ceramic Transactions, 92, 1 (1998).

Development of Mixed-Conducting Dense Ceramic Membranes for Hydrogen Separation, Proc. 5th Intl. Conf. Inorganic Membranes, Nagoya, Japan, June 22-26 (1998), 192-195.

Development of Proton-Conducting Membranes for Hydrogen Separation, presented at the Advanced Coal-based Power and Environmental Systems '98 Conference, Morgantown, WV, July 21-23, 1998.

The Effects of Dopants and A:B Site Nonstoichiometry on Properties of Perovskite-Type Proton Conductors, J. Electrochem. Soc., 145, 1780 (1998).

Transport Properties of $SrCe_{0.95}Y_{0.05}O_{3-a}$ and its Application for Hydrogen Separation, Solid State Ionics, 110, 303 (1998).

High-Temperature Deformation of $BaCe_{1-x}Y_xO_{3-y}$ ($0.05<x<0.2$), Solid State Ionics, 117, 323 (1999).

Development of Mixed-Conducting Ceramics for Gas Separation Applications, Mat. Res. Soc. Symp. Proc., 548, 545 (1999).

Performance Testing of Hydrogen Transport Membranes at Elevated Temperatures and Pressures, presented at Symposium on Hydrogen Production, Storage, and Utilization, New Orleans, Aug. 22-26, 1999; Am. Chem. Soc., Fuel Chem. Div., 44(4), 914 (1999).

Development of Mixed-Conducting Ceramic Membrane for Hydrogen Separation, presented at Sixteenth Annual International Pittsburgh Coal Conference, Pittsburgh, PA, Oct. 11-15, 1999.

Characterization of Ceramic Hydrogen Separation Membranes Containing Various Nickel Concentrations, presented at the Conference on Fossil Energy Materials -- Critical Supporting Technology R&D for Vision 21, Knoxville, TN, April 24-25, 2000.

Mixed Proton-Electron Conducting Cermet Membranes for Hydrogen Separation, presented at 102nd Annual Mtg. of the American Ceramic Society, St. Louis, MO, April 30-May 3, 2000.

Effect of Surface Modification on Hydrogen Permeation of Ni-$BaCeO_3$ Composites, presented at 102nd Annual Mtg. of the American Ceramic Society, St. Louis, MO, April 30-May 3, 2000.

Effect of Surface Modification on Hydrogen Permeation of Ni-$BaY_xCe_{1-x}O_{3-\delta}$ Composites, presented at 197th Meeting of the Electrochemical Society, Toronto, Ontario, Canada, May 14-19, 2000.

Evaluation and Modeling of a High-Temperature, High Pressure, Hydrogen Separation Membrane for Enhanced Hydrogen Production from the Water-Gas Shift Reaction, in "Advances in Hydrogen Energy," (Ed. C. E. G. Padro and F. Lau), Kluwer Academic/Plenum, New York, pp. 93-110 (2000).

Characterization of Ceramic Hydrogen Separation Membranes with Varying Nickel Concentrations, J. of Applied Surface Science, 167, 34 (2000).

The Crystal Structures and Phase Transitions in Y-doped $BaCeO_3$; Their Dependence on Y-Concentration and Hydrogen Doping, Solid State Ionics, 138, 63 (2000).

Development of Dense Ceramic Membranes for Hydrogen Separation, Proc. 26th International Conference on Coal Utilization and Fuel Systems, Clearwater, FL, March 5-8, 2001, pp. 751-761.

Thin-Film Cermet Membrane Preparation for Hydrogen Separation, presented at 103rd Annual Meeting of the American Ceramic Society, Indianapolis, IN, April 22-25, 2001.

Surface Modifications of Hydrogen-Separation Membranes Based on the Mixed Conductor Ni-BCY, presented at 103rd Annual Meeting of the American Ceramic Society, Indianapolis, IN, April 22-25, 2001.

Development of Dense Ceramic Membranes for Hydrogen Separation, published in the Proceedings of the 6th Natural Gas Conversion Symposium, Girdwood, Alaska, June 17-22, 2001.

Development of Dense Ceramic Membranes for Hydrogen Separation, Proceedings of the 18th International Pittsburgh Coal Conference, Newcastle, Australia, Dec. 4-7, 2001, published by the Pittsburgh Coal Conference, University of Pittsburgh, Pittsburgh, PA.

Defect Chemistry Modeling of High-Temperature Proton-Conducting Cerates, Solid State Ionics, 149, 1 (2002).

Current Status of Dense Ceramic Membranes for Hydrogen Separation, Proceedings of the 27th International Technical Conference on Coal Utilization and Fuel Systems, Clearwater, FL, March 4-7, 2002, published by the Coal Technology Association, Gaithersburg, MD.

Dense Ceramic Membranes for Hydrogen Separation, presented at the 16th Annual Conference on Fossil Energy Materials, Baltimore, MD, April 22-24, 2002.

Hydrogen Production by High-Temperature Water Splitting Using Mixed Oxygen Ion-Electron Conducting Membranes, Proc. 201st Electrochem. Soc. Mtg., Philadelphia, PA May-12-17 (2002).

Method for Generating Hydrogen by Catalytic Decomposition of Water, U. S. Patent #6,468,499, October 22, 2002.

Effect of Pd Coating on Hydrogen Permeation of Ni-Barium Cerate Mixed Conductor, Electrochemical and Solid-State Letters, 5(3), J5 (2002).

Electrical Properties of p-type Electronic Defects in the Protonic Conductor $SrCe_{0.95}Eu_{0.05}O_{3-d}$, Journal of Electrochemical Society, 150(6), A790 (2003).

Interfacial Resistances of Ni-BCY Mixed-Conducting Membranes for Hydrogen Separation, Solid State Ionics, 159, 121 (2003).

Defect Structure and n-Type Electrical Properties of $SrCe_{0.95}Eu_{0.05}O_{3-d}$, J. Electrochem. Soc., 150, A1484 (2003).

Hydrogen Production by Water Splitting Using Mixed Conducting Membranes, Proc. National Hydrogen Assoc. 14th Annual U.S. Hydrogen Meeting, Washington, DC, March 4-6, 2003.

Current Status of Mixed-Conducting Ceramic Membranes for Gas Separation Applications, presented at the Univ. of Houston, March 14, 2003.

Dense Cermet Membranes for Hydrogen Separation, presented at the 225th Amer. Chem. Soc. Natl. Mtg., Fuel Chemistry Div., New Orleans, March 23-27, 2003.

Hydrogen Production by Water Dissociation Using Mixed-Conducting Membranes, presented at 225th Amer. Chem. Soc. Natl. Mtg., Fuel Chemistry Div., New Orleans, March 23-27, 2003.

Current Status of Mixed-Conducting Ceramic Membranes for Gas Separation Applications, presented at the University of Illinois, Urbana-Champaign, April 24, 2003.

Hydrogen Production by Water Dissociation Using Oxygen-Permeable Cermet Membranes, presented at 105th Ann. Mtg. of Amer. Ceramic Soc., Nashville, April 27-30, 2003.

Preparation and Characterization of New Mixed Conducting Oxides $Ba(Zr_{0.8-x}Pr_xY_{0.2})O_{2.9}$, presented at 105th Ann. Mtg. of Amer. Ceramic Soc., Nashville, April 27-30, 2003.

Current Status of Dense Cermet Membranes for Hydrogen Separation, presented at the 20th Annual Intl. Pittsburgh Coal Conf., Pittsburgh, Sept. 15-19, 2003; in Conf. Proc., S46, 187.PDF, 2003.

Current Status of Ceramic Membranes for Hydrogen Production and Separation Applications, presented at the U. of Alaska-Fairbanks, Sept. 24, 2003.

Hydrogen Production by Water Dissociation Using Mixed Conducting Membranes, presented at Second Information Exchange Meeting on Nuclear Production of Hydrogen, Argonne Natl. Lab., Oct. 2-3, 2003.

A Method to Remove Ammonia using a Proton-Conducting Membrane, U.S. Patent #6,630,116, Oct. 7, 2003.

Numerical Modeling of Hydrogen Permeation in Chemical Potential Gradients, Solid State Ionics, 164, 107 (2003).

Development of Dense Cermet Membranes for Hydrogen Separation, presented at the 204th Mtg. of the Electrochemical Soc., Orlando, Oct. 12-17, 2003.

Hydrogen Permeation of Cermet $Ba(Ce_{0.6}Zr_{0.2})Y_{0.2}O_3$/Ni Membranes, presented at the 204th Mtg. of the Electrochemical Soc., Orlando, Oct. 12-17, 2003.

Hydrogen Permeability of $SrCe_{1-x}M_xO_{3-d}$ (x = 0.05, M = Eu, Sm), Solid State Ionics, 167, 99 (2004).

Use of Mixed Conducting Membranes to Produce Hydrogen by Water Dissociation, Intl. Journal of Hydrogen Energy, 29, 291-296 (2004).

Hydrogen Production from Water Splitting Using Mixed Oxygen-Electron Conducting Membranes, U. S. Patent #6,726,893, April 27, 2004.

Hydrogen Production by Water Dissociation using Mixed-Conducting Ceramic Membranes, Proc. of National Hydrogen Assoc. 15th Annual U.S. Hydrogen Energy Conf., Los Angels, CA, April 27-30 (2004).

Mixed-Conducting Dense Ceramic Membranes for Hydrogen Production and Separation from Methane, presented at 15th World Hydrogen Energy Conf. Yokohama, Japan, June 27-July 2 (2004).

Hydrogen Production from Water Using Mixed-Conducting Ceramic Membranes, presented at 15th World Hydrogen Energy Conf. Yokohama, Japan, June 27-July 2 (2004).

Development of Dense Ceramic Membranes for Hydrogen Production and Separation, Proc. of 8th Intl. Conf. on Inorganic Membranes, Ed. by F. T. Akin and Y. S. Lin, Adams Press, Chicago, IL (2004) Pgs. 163-166.

Development of Dense Cermet Membranes for Hydrogen Separation, presented at 21st Annual Intl. Pittsburgh Coal Conf., Osaka, Japan, Sept. 13-17 (2004).

Hydrogen Permeation of Cermet [Ni-$Ba(Ce_{0.6}Zr_{0.2})Y_{0.2}O_{3-a}$] Membranes, presented at the 206th Mtg. of the Electrochemical Soc., Honolulu, Oct. 3-8, 2004.

Development of Dense Ceramic Membranes for Hydrogen Production and Separation, presented at American Soc. for Materials-Annual Materials Solution Conf., Columbus, OH, Oct. 18-21 (2004).

Electrical and Hydrogen Transport Properties of $SrCe_{0.8}Yb_{0.2}O_{3-d}$/Ni Cermet Membranes, presented at Fall Meeting of Materials Research Society, Boston, Nov. 29-Dec. 3 (2004).

Preparation and Hydrogen Pumping Characteristics of $BaCe_{0.8}Y_{0.2}O_{3-d}$ Thin Film, presented at Fall Meeting of Materials Research Society, Boston, Nov. 29-Dec. 3 (2004).

Hydrogen Permeability and Microstructure Effect of Mixed Protonic-Electronic Conducting Eu-Doped Strontium Cerate, J. Mater. Sci., 40, 4061-4066 (2005).

Defect Structure and Transport Properties of Ni-$SrCeO_{3-d}$ Cermet for Hydrogen Separation Membrane, Submitted to J. Electrochem. Soc. 152(11) J125 (2005).

Dense Cermet Membranes for Hydrogen Separation, Presented at American Institute of Chemical Engineers (AIChE) Spring National Meeting, Atlanta, GA, April 10-14, 2005.

Hydrogen Separation Using Dense Cermet Membranes, presented at 30th Intl. Tech. Conf. on Coal Utilization and Fuel Systems, Clearwater, FL, April 17-21, 2005.

Development of Dense Ceramic Membranes for Hydrogen Separation, presented at 2005 DOE Annual Hydrogen Program Review, Washington, DC, May 23-25, 2005.

Mixed-Conductors for Electric Power Applications, Presented at NANOMAT-Birkeland Conf., Trondheim, Norway, June 2-3, 2005.

Membranes: The Good, The Bad, and The Ugly, presented to Hydrogen & Fuel Cell Tech. Prog. Office, DOE, Wash., DC, June 8, 2005.

Thin Film Preparation and Hydrogen Pumping Characteristics of $BaCe_{0.8}Y_{0.2}O_{3-\delta}$, Solid State Ionics, 176, 1479-1484 (2005).

Hydrogen Production by Water Splitting Using Dense Thin-Film Cermet Membranes, presented at Fall Meeting Materials Research Society, Boston, Nov.28-Dec. 2, 2005.

Hydrogen Permeation and Chemical Stability of Cermet [Ni-$Ba(Zr_{0.8-x}Ce_xY_{0.2})O_3$] Membranes, Electrochem. & Solid State Letts., 8(12), J35-J37 (2005).

Electrochemical Hydrogen Pumping Characteristics of $BaCe_{0.8}Y_{0.2}O_{3-\delta}$ Thin Film, presented at Electrochem. Soc. 2005 Fall Mtg., Los Angeles, Oct. 16-21, 2005.

Hydrogen Production by Water Dissociation Using Mixed Oxygen Ion-Electron Conducting Membranes, presented at Electrochem. Soc. 2005 Fall Mtg., Los Angeles, Oct. 16-21, 2005.

Hydrogen Permeation of Ceramic/Metal Composite Thin Films, presented at Electrochem. Soc. 2005 Fall Mtg., Los Angeles, Oct. 16-21, 2005.

Development of Dense Cermet Membranes for Hydrogen Separation, Invited presentation at World Hydrogen Technologies Convention, Singapore, Oct. 3-6, 2005.

Review: Stress-Induced Diffusion and Cation Defect Chemistry Studies of Perovskites, Invited paper to be published in "Defects & Diffusion in Ceramics - Annual Retrospective 2005; Defect & Diffusion Forum," published by Scitec Publication, London, UK (Oct. 2005).

Mixed-Conducting Dense Ceramic Membranes for Air Separation and Natural Gas Conversion, J. of Solid State Electrochemistry, 10, 617-624, (2006).

Hydrogen Production by Water Dissociation Using Mixed Conducting Dense Ceramic Membranes, Intl. J. of Hydrogen Energy (in press, 2006).

Hydrogen Separation by Dense Cermet Membranes, Fuel, Vol. 85(2), 150-155 (2006).

Hydrogen Production by Water Dissociation Using Mixed-Conducting Dense Ceramic Membranes, Invited presentation at Amer. Chem. Soc. 231st Natl. Mtg., Atlanta, March 26-30, 2006.

Development of Dense Cermet Membranes for Hydrogen Separation, presented at AIChE Spring Mtg., Orlando, FL, April 23-27 (2006).

Method for Fabricating a Hydrogen Separation Membrane on a Porous Substrate, Patent Application, filed May 5, 2006.

Thermal Method for Fabricating a Hydrogen Separation Membrane on a Porous Substrate, Patent Application, filed May 5, 2006.

Method for Fabricating Dense Thin Film Cermet Hydrogen Separation Membrane, Patent Application, filed May 5, 2006.

Hydrogen Production from Methane Using Dense Oxygen and Hydrogen Transport Membranes, presented at 209th Electrochemical Soc. Mtg., Denver, May 7-12, 2006.

Development of Dense Hydrogen Transport Membranes, presented at the 31st International Technical Conference on Coal Utilization and Fuel Systems, Clearwater, FL, May 21-25, 2006.

Mixed-conducting Membranes for Hydrogen Production and Separation, presented at 2006 MRS Fall Meeting, Boston, MA, Nov 27 - Dec 1, 2006.

REFERENCES

1) U. Balachandran et al., Argonne National Laboratory Hydrogen Separation Membranes-Quarterly Report for January-March 2006. (3-7/06)

2) U. Balachandran et al., Argonne National Laboratory Hydrogen Separation Membranes-Annual Report for FY 2005. (1-4/06)

3) U. Balachandran et al., Argonne National Laboratory Hydrogen Separation Membranes-Annual Report for FY 2000. (4-7/06)

4) ASME Boiler Code (2004) and Case #2385-1 (ESH Plan for High-Pressure reactor).

5) "Hydrogen Safety Manual" (published in 1983 by the Commission of the European

6) John C. Molburg and Richard D. Doctor, *Comparative Economics of Hydrogen and Electricity from Shell-IGCC using High-Sulfur and Low-Sulfur Coals with CO_2 Capture*, 22nd Annual International Pittsburgh Coal Conference, Pittsburgh, PA 12-15 September 2005.

7) U. Balachandran et al., Argonne National Laboratory Hydrogen Separation Membranes-Quarterly Report for April-June 2006. (new)

8) J. R. Taylor, Met. Trans., Vol. 16B, 143-148 (1985). (6-7/06)

9) O. Knacke, O. Kubaschewski, and K. Hesselmann, Thermochemical Properties of Inorganic Substances I, 2nd Ed., Springer-Verlag, Berlin (1991).

10) T.H. Lee, S.E. Dorris, and U. Balachandran, Solid State Ionics, 176 (2005) 1479.

11) U. Balachandran, T.H. Lee, S. Wang, and S.E. Dorris, Int. J. Hydrogen Energy, 29, 291 (2004).

12) U. Balachandran et al., Argonne National Laboratory Hydrogen Separation Membranes-Annual Report for FY 2004. (1-10/06Tae)

13) U. Balachandran, T.H. Lee, S. Wang, and S.E. Dorris, Hydrogen Production by Water Dissociation Using Mixed Conducting Dense Ceramic Membranes, Int. J. Hydrogen Energy (in press). (2-10/06Tae)

14) U. Balachandran, Argonne National Laboratory Hydrogen Separation Membranes-Quarterly Report for October-December 2004.

Energy Systems Division
Argonne National Laboratory
9700 South Cass Avenue, Bldg. 212
Argonne, IL 60439-4838

www.anl.gov

UChicago ▶ Argonne LLC

A U.S. Department of Energy laboratory
managed by UChicago Argonne, LLC